Strategic Planning and Deployment of Aerial Assets

by

Akila Saravanan

B.S. in Computer Science and Aeronautics and Astronautics, MIT, 2023

Submitted to the Department of Aeronautics and Astronautics
in partial fulfillment of the requirements for the degree of

MASTERS OF SCIENCE IN AERONAUTICS AND ASTRONAUTICS

at the

MASSACHUSETTS INSTITUTE OF TECHNOLOGY

May 2024

Authored by:	Akila Saravanan Department of Aeronautics and Astronautics May 17, 2024
Certified by:	Hamsa Balakrishnan William E. Leonhard Professor of Aeronautics and Astronautics, Thesis Supervisor
Accepted by:	Jonathan How R. C. Maclaurin Professor of Aeronautics and Astronautics Chair, Graduate Program Committee

Strategic Planning and Deployment of Aerial Assets

by

Akila Saravanan

Submitted to the Department of Aeronautics and Astronautics
on May 17, 2024 in partial fulfillment of the requirements for the degree of

MASTERS OF SCIENCE IN AERONAUTICS AND ASTRONAUTICS

ABSTRACT

The rapid deployment of fleets of small, uncrewed aircraft (drones) for tasks like package delivery or search-and-rescue in the immediate aftermath of a natural disaster are some of the most vital and common applications of advanced air mobility. Recognizing that successful drone missions depend on pre-established, well-positioned bases and efficient task allocation, this work presents a generalizable model for base positioning and routing in diverse applications. The proposed model prioritizes choosing bases that both maximize operational coverage and enable rapid responses to high-demand areas. Additionally, the framework integrates a vehicle routing component to optimize drone flight paths for efficient task completion in the tactical portion of drone-based operations; this component is the primary focus of this work. In addition to the theoretical formulation, the models are validated through case studies examining post-flooding search-and-rescue in the Iwate prefecture of Japan and package deliveries in the Austin, TX metropolitan area.

Thesis supervisor: Hamsa Balakrishnan
Title: William E. Leonhard Professor of Aeronautics and Astronautics

Acknowledgments

First and foremost, I would like to thank my research advisor, Professor Hamsa Balakrishnan. For the past 5 years, since my freshman year, I've benefited immensely from her guidance, expertise, and unwavering support. Her mentorship solidified my passion for research and helped me navigate my path as a researcher. I particularly appreciate the numerous opportunities she provided me throughout my time in her lab, from exploring new areas of research to publishing and presenting my work. These opportunities have fostered my growth as a problem solver.

Special recognition goes to Dr. Karthik Gopalakrishnan and Dr. Chris Chin. Despite their demanding PhD schedules, they consistently made time to assist me with troubleshooting code and exploring alternative solutions when I got stuck. I extend my gratitude to the entire DINaMo lab, where everyone has been a source of inspiration during the past five years. It is always great to be around a set of people who are inspirational in their intelligence and work ethic but equally fun-spirited (as evident during lab holiday parties).

I am grateful to the MIT Department of Aeronautics and Astronautics and the Benjamin P. and Margaret Blasingame Fund for awarding me an academic fellowship. This support allowed me to stay fully dedicated to my research without additional academic commitments.

Finally, my deepest appreciation goes to my family and friends. Mom, Dad, grandparents, and my extended MIT family (special shoutout to MIT Sport Taekwondo and the MIT Ohms) – their unwavering love and support have been essential throughout this entire journey. Whether it was acting as my rubber ducky during debugging sessions or bringing me ice cream during late nights, their encouragement, in all its forms, fueled my success.

Contents

List of Figures

List of Tables

Chapter 1

Introduction

The past decade has witnessed a significant surge in the development of Advanced Air Mobility (AAM) systems, particularly focusing on small, uncrewed aircraft (drones). This growth is fueled by advancements in battery technology, miniaturization of electronics, and increased affordability of these systems. These advancements have opened doors to many AAM applications, impacting various sectors and offering innovative solutions to existing challenges. Search-and-rescue missions in the aftermath of natural disasters and last-mile delivery services in urban environments are two prominent examples of this. However, the effectiveness of these operations hinges on two core factors:

1. **Strategic base placement:** Drones require well-positioned bases to ensure efficient deployment, rapid response times, and adequate operational coverage.

2. **Optimized task allocation and routing:** Once deployed, drones need a system for efficiently allocating tasks and planning flight paths to maximize operational efficiency and minimize completion time.

This work addresses these challenges by proposing a generalizable model for drone base station positioning and routing, applicable to diverse applications. Beyond the theoretical framework, the model is validated through two case studies examining:

1. Post-flooding search and rescue

2. Urban package delivery

1.1 Background

1.1.1 Search and Rescue

One of the most captivating applications of AAM lies in its potential to revolutionize disaster response efforts. The number of natural disasters experienced worldwide per decade has increased five-fold over the past 50 years, driven primarily by climate change and extreme weather [1]. Rising temperatures and warmer seas cause more water vapor to evaporate into the atmosphere, fueling storms like hurricanes, typhoons, and torrential rain. At the same time, urbanization and population growth have limited the area that can be used for water absorption after intense rains. Recent studies suggest that these factors compound and make floods the most common meteorological hazard, causing numerous casualties and significant property damage. In Japan, for example, approximately 41% of the population and 65% of national assets are concentrated in flood-prone areas [2], [3].

Large-scale natural disasters such as floods and earthquakes often disrupt ground infrastructure such as road networks, necessitating the use of alternative modes of sensing and transport for disaster response [4]. Damaged roads, debris-filled landscapes, and hazardous environments can hamper traditional search-and-rescue methods. Drones offer a unique advantage in such scenarios. Their ability to navigate complex terrain, access remote areas, and provide aerial imagery can significantly improve search efficiency and expedite rescue efforts.

The 2011 Tohoku earthquake and tsunami in Japan serves as a poignant example of the challenges faced in disaster response. Widespread damage to infrastructure and the Fukushima Daiichi nuclear power plant crisis made traditional rescue efforts on the ground incredibly difficult. Drones, however, played a crucial role in damage assessment, exploring regions that can not be traversed by humans [5]. In the US, UAV use in disaster response dates back to 2005, when Texas A&M Center for Robot-Assisted Search and Rescue

(CRASAR) used UAVs to search for Hurricane Katrina survivors in Mississippi. Since then, drones have been used in other similar disaster situations like Hurricane Harvey and Ian for search and rescue operations, damage assessment, and delivery of aid [6], [7]. These instances solidify the crucial role drones can play in saving lives and accelerating recovery efforts in the aftermath of natural disasters.

However, traditional search-and-rescue methods still rely heavily on aerial imaging using conventional helicopters. While these provide valuable information, clear images are rarely available in real-time due to operational constraints, tasking limitations of satellites, and occlusions such as clouds [8]. Advances in autonomy, the commercialization of small drones, and new imaging technologies have made drone-based aerial sensing a growing part of post-disaster search operations [9], [10].

1.1.2 Urban Package Deliveries

Beyond disaster response, AAM holds significant promise in transforming urban logistics and delivery services. The rise of e-commerce and the growing demand for same-day delivery have strained traditional ground-based transportation systems, particularly in densely populated urban areas [11]. Drones offer a compelling alternative by enabling last-mile delivery solutions that bypass traffic congestion and expedite delivery times.

While the potential of AAM in urban package delivery is attractive, challenges persist. Regulations regarding drone operation in urban environments are still evolving, encompassing concerns surrounding airspace management, safety, noise pollution, and privacy [12]. Additionally, battery life limitations on current drone models restrict operational range and payload capacity [13].

Several companies are actively exploring and developing drone delivery solutions, pushing the boundaries of this technology. Companies like Amazon, Alphabet's Wing, and UPS are conducting pilot projects in various locations around the world, testing the feasibility and efficiency of drone delivery services [14]. These programs serve as real-world testing grounds,

allowing them to assess the feasibility, efficiency, and challenges associated with large-scale drone delivery operations [15]. Companies like UPS Flight Forward are also entering the space, collaborating with healthcare providers to explore drone delivery for critical medical supplies [16].

Despite the promising potential of drone delivery, several challenges remain to be addressed before widespread adoption can occur. These challenges, particularly in the context of route planning and resource allocation, include:

1. **Battery Life and Range:** Unfortunately, current UAV delivery has a limited range (distance and flight time) and capacity (weight and size), so they often can not deliver all the packages in a single trip. To overcome these limitations, deploying multiple drones to split the workload or incorporating strategic recharging stops in single trip or between trips will be necessary. Optimization algorithms are crucial to design efficient routes that maximize deliveries within these battery constraints.

2. **Urban Air Traffic Management:** Efficient drone delivery requires robust air traffic management systems to ensure safe and conflict-free operation in urban airspaces. Route planning algorithms need to consider potential restrictions and obstacles.

3. **Computational Efficiency:** As the number of drones and delivery locations increases, route planning algorithms need to be computationally efficient to generate optimal or near-optimal solutions in real-time.

4. **Customer Preferences and Delivery Windows:** Delivery routes need to factor in customer preferences for delivery times and locations, while maintaining optimal routes.

1.2 Literature Review

There has been considerable work on the efficient distribution of tasks among drones, along with the optimization of their trajectories [17]–[19]. Optimization techniques such as dynamic vehicle routing [20]–[22] and neuro-fuzzy dynamic programming [23] have been proposed in this context. Large-scale optimization formulations have also been developed [24], [25]. Recent work has also focused on drone trajectory and mission assignment optimization [18]. Strategic disaster response planning [26] and base location problems [27] have similarities to those of aircraft base location [28], air ambulance base location planning [29], [30], set covering [31], and generalized facility location problems [32]. To make an easily generalizable model, this work focuses on traditional optimization methods that are not use-case specific.

Achieving efficient last-mile delivery presents a significant challenge in the growing e-commerce landscape. The final leg of the supply chain (last-mile delivery) is the most expensive and time-consuming segment, directly impacting customer satisfaction and a company's bottom line [33]. Inefficient routing due to poorly planned delivery networks significantly contributes to this issue. An in-depth literature review by Ha, Akbari, and Au identifies five core dimensions of the "last-mile" problem - last-mile operations, transportation, delivery, distribution, and logistics. These 5 elements require a combination of operational, tactical, and strategic methods [33]. Several papers explore solutions for this, highlighting the importance of strategic base location selection. Many also examine how basing delivery vehicles closer to warehouses reduces travel times and optimizes routes through mathematical modeling [34]. This proximity fosters efficiency and agility. Delivery personnel can respond faster to customer requests within a designated service area. Furthermore, studies like [35] examine the impact of alternative routing strategies on factors like distance traveled, delivery time, equity, and even environmental impact. By strategically placing bases closer to warehouses and customer clusters, companies can leverage these findings to design delivery networks that are efficient and also address individual priorities. The flexibility to optimize

individual priorities is emphasized in much of the literature and is a feature we consider in the development of models for this work (equity of access to help in the SAR case and timely action in the delivery case).

Equity of access, i.e., whether all regions or groups of people are being served fairly, needs to be an important aspect of any public service, more so a life-saving one such as search-and-rescue [36]. Transportation equity research has primarily focused on the potentially regressive impacts of pricing mechanisms [37]–[40]. However, with the growth of dynamic demand and on-demand services, the issue of equity in access to services has become a growing concern that needs to be addressed [41].

Existing research on routing problems for Search and Rescue (SAR) operations and drone deliveries has leveraged both Vehicle Routing Problems (VRPs) and Traveling Salesman Problems (TSPs) to great effect[42], [43]. VRPs demonstrably improve route optimization by considering capacity constraints in multi-stop scenarios. However, their computational complexity increases significantly with large datasets, which can hinder real-time decision-making in applications like SAR operations [44].

On the other hand, vanilla TSPs offer faster computation times but struggle to incorporate real-world complexities. Some works have begun to look at more complex modifications to TSPs, specifically for civil applications, but more involved extensions like accounting for urgency levels in SAR missions or noise and privacy constraints in an urban environment that delivery drones must abide by have not yet been focused on [45]. Furthermore, existing research often purely focus on minimizing total distance traveled, though there are some variations like TSPs with Time Windows that are designed to account for weather uncertainty [46]. However, factors like privacy and noise constraints, terrain difficulty, and resource limitations that can significantly influence search efficiency or delivery success are not fully addressed. Handling these limitations by varying the prioritizes and constraints of TSPs and VRPs can provide alternative routing algorithms that consider these real-world complexities. This will be crucial for developing more robust and adaptable solutions for

both SAR and drone delivery applications.

We draw from much of this literature in developing optimization formulations for strategically locating drone bases and prioritizing search order, taking into account the probability of search need and operational constraints.

1.3 Thesis Objectives

This thesis tackles the challenge of optimizing drone base placement and operation strategies. Our focus is twofold. The first objective is to determine the most effective locations for drone bases within a designated region. This strategic placement aims to maximize the area covered by drones while minimizing the time it takes them to reach various locations. This is particularly critical for search-and-rescue (SAR) operations where rapid deployment of drones can save lives.

The second objective revolves around developing algorithms that plan efficient flight paths for drones dispatched from the selected bases. These algorithms will consider various factors to optimize drone operations. Minimizing total travel time and ensuring efficient resource utilization are key priorities. Additionally, the algorithms will account for the limited flight range of drones, ensuring they remain within operational boundaries.

This work focuses on real-world scenarios and acknowledges the limitations these bring, such as resource restrictions. For example, the number of available bases could be restricted by personnel and drone availability for SAR operations. It also addresses situations where complete regional coverage with drone bases might not be achievable. In such cases, our work aims to strategically position bases to prioritize areas with the highest likelihood of requiring drone assistance, such as post-disaster rescue zones or zones with high package demand (hospitals for medical supplies, large office spaces, etc).

The focus of this work is the exploration and implementation of various vehicle routing models to plan the paths of drones from their bases to various search locations. These

vehicle routing models range from Vanilla Travelling Salesman Problems (TSPs) and Prize-Collecting Travelling Salesman Problems (PCTSPs) to Capacitated Vehicle Routing Problems (CVRP) depending on the use case.

The effectiveness of the proposed framework is evaluated through two case studies:

1. SAR Drone Fleet for Flood Evacuation in Iwate, Japan: This case study will simulate drone deployment for rescuing flood evacuees in Iwate prefecture.

2. Package Delivery in Metropolitan Areas: The framework will be applied to optimize delivery routes for drone fleets in the urban areas of Austin, TX.

Chapter 2

Phase 1: Choosing Base Locations

This phase was developed for the search-and-rescue case study and adapted for the drone delivery case study. As such, the following sections will focus on the search-and-rescue scenario and a brief section will cover the adaptation.

2.1 Problem Setup

2.1.1 Search-and-Rescue Operations

We study the Iwate prefecture, which is the second largest prefecture in Japan, with an area of over 15,000 square kilometers. As of 2020, the Iwate prefecture ("Iwate") had a population of 1.2 million and had the lowest population density of any prefecture on Japan's main island, Honshu [47]. Fig. 2.1 shows the location and extent of Iwate. Many of its larger cities/towns lie in the Kitakami River valley, running vertically through the western half of Iwate. The coastal areas on the east also contain cities with more than 50,000 people, such as Kitakami and Miyako.

Like much of Japan, Iwate is susceptible to natural disasters, including earthquakes, tsunamis, and flooding. The March 2011 Tohoku earthquake, also referred to as the "Great East Japan Earthquake" was the most powerful earthquake recorded in Japan (and also the

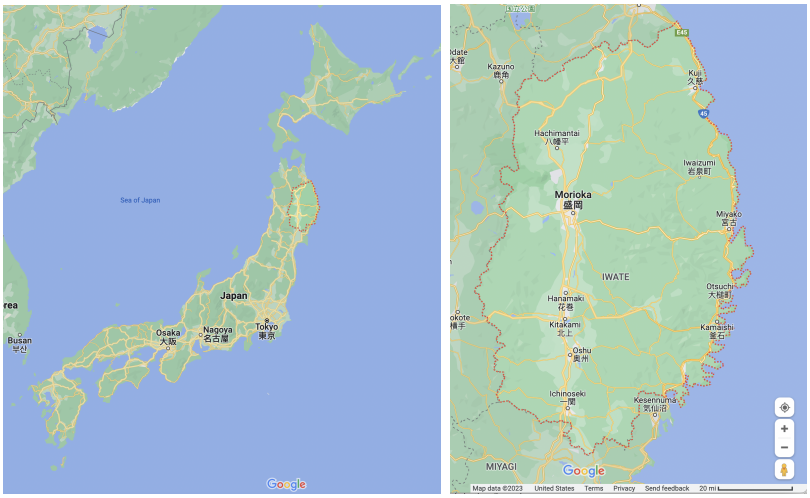

Figure 2.1: (Left) Map of Japan with Iwate prefecture shown within the red dotted line, and (Right) zoomed-in map of Iwate prefecture.

precursor to the infamous Fukushima accident) [48]. The coastal areas of Iwate were heavily impacted—tsunami waves triggered by the earthquake reached up to 40 meters (131 feet) in Iwate's coastal city of Miyako [49]. With over 15,000 deaths and $220 billion USD in damage, the Tohoku earthquake was the costliest natural disaster in world history [50]. As a rural area susceptible to natural disasters, Iwate is conducive to deploying drones for disaster response. According to experts from JAXA and local government officials, drones would perform round-trip search and reconnaissance ("search") flights from pre-defined bases. The location of these bases will impact their effectiveness; bases far away from areas requiring search would hamper operations. Locating bases as close as possible to potential search areas is insufficient, as other objectives need to be considered. For example, before a disaster, the areas with search needs are uncertain, so it is important to place bases so they can cover large parts of the prefecture.

Input data

We divide Iwate into 15,452 1-km×1-km cells, denoted by the set I. We identified the set of candidate base locations J by consulting local experts. We assume that at most P number of bases can be opened. Since the range of drones deployed is uncertain, we assume that

drones can search cells within a maximum distance L km of a base. At the time that base location decisions are made, we assume that for each cell i we have an estimated probability p_i that cell i will need to be searched. We estimate these probabilities based on four layers of spatial data: elevation, population, flooding locations, and rescue mission locations. As a disaster approaches, more detailed data (e.g., real-time weather maps) could be used. But our formulations for base locations do not depend on how the search need probabilities are generated.

We used the *Open Topo Data* API and the 30m SRTM database to get open-source elevation and population data. We defined the elevation of each cell as that of the centroid of each cell. A heat map of elevations in Iwate can be seen in Fig. 2.2a. The lighter pink colors correspond to areas of lower elevation. We used population data (obtained from the Iwate prefecture official website) for the 31 cities/towns in Iwate that are independent local government units. To identify areas of potential flooding, we used an existing JAXA hazard-risk area assessment. These largely correspond to the eastern coastal areas, as shown in Fig. 2.2c.

The rescue location data is based on scenarios generated by JAXA. One of the main challenges in disaster response planning is the limited availability of data. Because of privacy issues, information on the location and number of evacuees, for example, is only sporadically released. Data on rescue missions performed are typically only released in summary reports. JAXA's rescue mission database includes rescue locations and the number of evacuees at these locations. Data from past disasters, particularly the Great East Japan Earthquake and Tsunami, were used in the creation of the scenarios. JAXA also relied on interviews with local rescue authorities and input from subject-matter experts. Flight reports were obtained from local fire departments, medical assistance teams, homeland protection, police departments, and the coast guard. JAXA conducted interviews with pilots and rescue personnel involved in the relief mission to verify assumptions. The modeled rescue locations are shown in Fig. 2.2d.

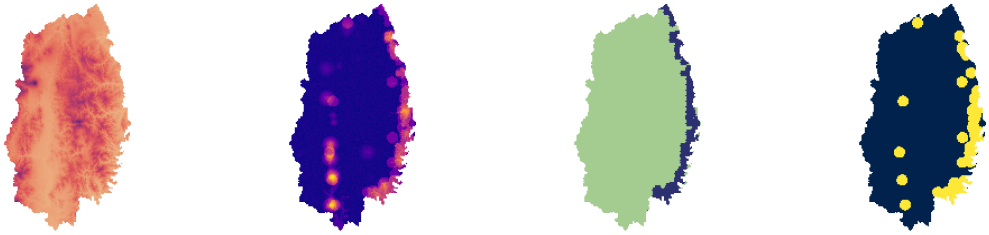

(a) Elevation (lighter colors indicate lower elevation).

(b) Population (lighter colors indicate higher population).

(c) Flooding areas (in blue)

(d) Prior rescue locations (in yellow).

Figure 2.2: Inputs used to estimate the probability of search need for each cell in Iwate prefecture.

Probabilities of needing search

Based on the input data layers, we then estimate the search need probability ("search probability") for each cell. This represents the probability that a cell will need to be searched during disaster response, i.e., that the cell might contain someone who needs to be rescued. The probability weightings and thresholds are not meant to be exact; rather, they provide us with a starting point from which to illustrate the base location process. Increasing the accuracy of estimated search probabilities is an important topic but not the focus of this paper. We use the following procedure:

- **Initialization:** We initialize the probability of each cell using a uniform distribution in the range (0, 0.05).
- **Elevation:** We set 50 m (164 ft) as the elevation threshold. We increase the probability of the 603 cells with elevation less than this by 0.15.
- **Population:** We adjust cells based on nearby cities and towns. We set the city threshold as 8 km and the town threshold as 4 km. Cells within that threshold of a city/town had their probabilities increased by between (0, 0.25). For a given city/town we differentiate the probability increase of cells based on the distance from the city/town to the cell and the city/town population. Cells closest to large populations see the greatest

increase in probability.

- **Prior flooding:** We set 3 km as the flooding threshold. Cells that lie within this threshold of a flooding location have their probability of search need increase by 0.25. This affects 1,413 cells.

- **Rescue:** We set 5 km as the rescue threshold. We increase the probability of the 1,976 cells within this threshold of a rescue location by 0.3.

Fig. 2.3 shows our estimated search probabilities. There is a high concentration of high-probability areas on the eastern coast. These low-elevation areas contain flooding and rescue locations. In the western half of Iwate, there is a vertical strip of higher probability area, which corresponds to the densely populated Kitakami River Valley in Iwate. The candidate base locations are indicated with squares. They are all independent local government units in Iwate Prefecture. Besides being more capable of supporting drone operations, these locations are typically used as ad hoc disaster response operations centers.

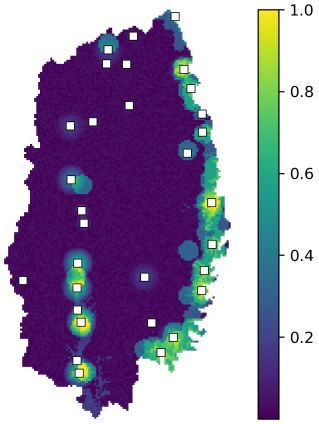

Figure 2.3: Estimated probabilities of search need, with candidate base locations indicated by white square icons.

2.1.2 Optimizing Base Locations

Baseline Formulation

We first consider two priorities in base location: 1) maximizing coverage of the Iwate prefecture, and 2) minimizing the distance between bases and high-probability search areas. We use the following notation:

Sets

I: set of Iwate cells, indexed by i

J: set of candidate base locations, indexed by j

Parameters

p_i: probability of cell i needing search

d_{ij}: distance from cell i to base j

L: maximum distance between base and cell it serves

B_i: set of eligible bases within distance L of cell i

P: maximum number of bases

Decision Variables

$$x_j = \begin{cases} 1, & \text{if base } j \text{ is opened} \\ 0, & \text{otherwise} \end{cases}$$

$$z_i = \begin{cases} 1, & \text{if cell } i \text{ is covered} \\ 0, & \text{otherwise} \end{cases}$$

$$y_{ij} = \begin{cases} 1, & \text{if cell } i \text{ is covered and has closest base } j \\ 0, & \text{otherwise} \end{cases}$$

We consider a cell i to be "covered" if a base within distance L is open. Note that we also tested a formulation with base vehicle capacity constraints, but the locations generally did not change. The objective can be written as follows:

$$\max \ \alpha \sum_{i \in I} p_i z_i - \beta \sum_{i \in I} \sum_{j \in B_i} p_i d_{ij} y_{ij}$$

The first term of the objective rewards cells being covered by bases (we call this "coverage"). It is more rewarding to cover cells with a higher probability of search need. The second term minimizes the weighted distance between covered cells and their closest open base. The α and β coefficients indicate the trade-off between maximizing coverage and minimizing the distance to the nearest bases. As coverage increases, base locations will be more dispersed throughout Iwate, increasing the weighted distance between cells and open bases.

To simplify notation, we set $\alpha = 1$ and define $\gamma = \beta/\alpha$, as shown in expression (2.1). If $\gamma = 0$, the objective solely focuses on maximizing coverage. On the other hand, as γ goes to infinity, the second term of the objective dominates. This can lead to solutions where no bases are located with an objective value of 0. On an individual cell level, a cell i will not be covered if the distance penalty (second term of the objective) outweighs the coverage benefit (first term). In terms of variables, $z_i = 0$ if $\gamma > 1/d_{ij} \ \forall j \in B_i \cap \{j \in J | x_j = 1\}$. To avoid this issue, we specify $\gamma \leq 1/L$, since the maximum distance between a base and a cell it serves is L.

Constraint (2.2) sets the maximum number of bases to be located. Constraint (2.3) ensures that a cell is only counted as "covered" (denoted by z) if a base within L distance of it is opened (denoted by x). Constraint (2.4) relates z and y decision variables. If a cell is covered, then there exists at least one closest base (indicated by y). Constraint (2.5) helps define y_{ij}, which can only take a value of 1 if base j is opened. That is, a base j needs to be open for it to serve a cell i. Constraint (2.6) stipulates that each cell has at most one closest base.

$$\max \sum_{i \in I} p_i z_i - \gamma \sum_{i \in I} \sum_{j \in B_i} p_i d_{ij} y_{ij} \tag{2.1}$$

$$s.t. \quad \sum_{j \in J} x_j \leq P \tag{2.2}$$

$$z_i \leq \sum_{j \in B_i} x_j \quad \forall i \in I \tag{2.3}$$

$$z_i \leq \sum_{j \in B_i} y_{ij} \quad \forall i \in I \tag{2.4}$$

$$y_{ij} \leq x_j \quad \forall i \in I, j \in B_i \tag{2.5}$$

$$\sum_{j \in B_i} y_{ij} \leq 1 \quad \forall i \in I \tag{2.6}$$

$$x_j, z_i, y_{ij} \in 0, 1 \quad \forall i, j \tag{2.7}$$

We fixed $\gamma = \frac{1}{5L}$ and varied P and L. Fig. 2.4 displays four coverage maps for different P and L values that made most sense for the experiments we modeled. The yellow "X" marks indicate the chosen base locations. Cells that are colored light grey are "uncovered", meaning that their nearest base is more than L distance away. Cells that are colored the same share the same nearest base; for example, the orange points in Fig. 2.4a share the base in the southwestern part of Iwate. The subfigure captions indicate the values of P and L used, and the coverage and mean distance to nearest base (DNB) is shown on top of each subfigure. We display results for various combinations of $P = 3, 4, 5$ and $L = 40, 50$. As the number of bases or the radius L increases, more cells are covered. As P increases, the mean DNB generally decreases, as cells have more viable bases that can cover them.

Uncertainty in base availability

In the previous subsection, we focused on applying the basic formulation from our previous paper [51], which assumes that chosen base locations will be operable immediately following

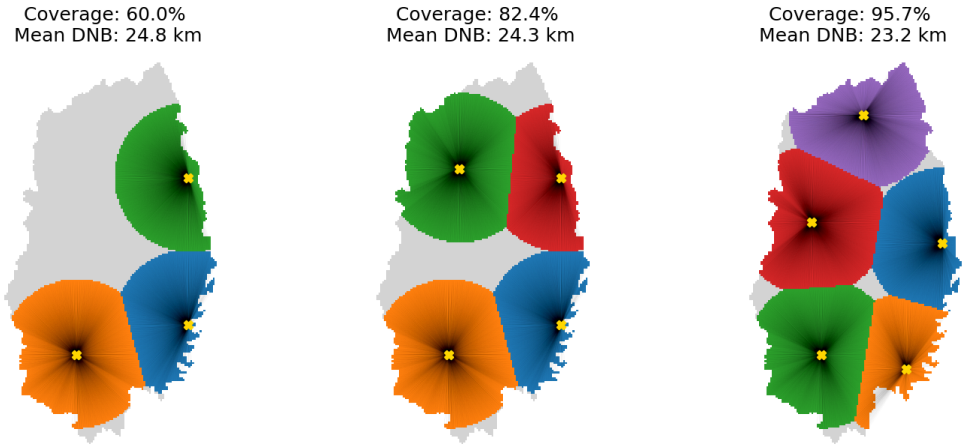

(a) P=3, L=40 km (b) P=4, L=40 km (c) P=5, L=40 km

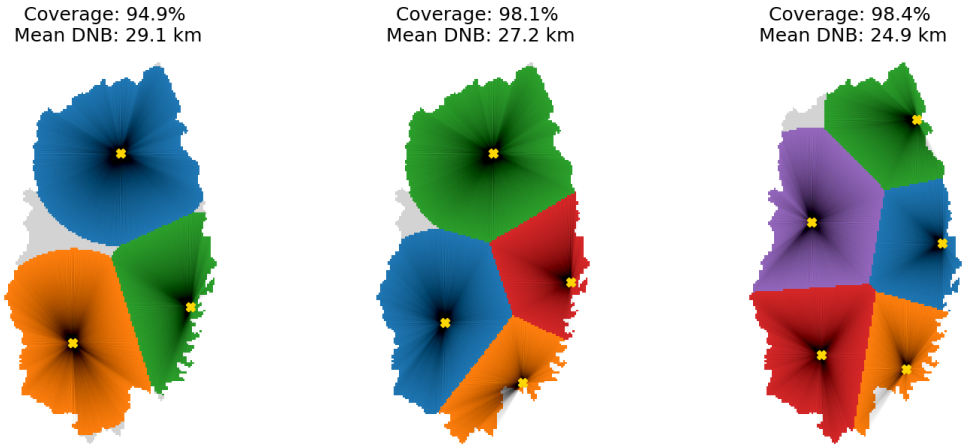

(d) P=3, L=50 km (e) P=4, L=50 km (f) P=5, L=50 km

Figure 2.4: Effect of varying the number of bases (P) and the maximum distance reachable from a base, L, when $\gamma = \frac{1}{5L}$. Coverage indicates the percentage of cells covered, and DNB stands for distance from a cell to the nearest base.

a disaster. This may not always be the case, as some of the base locations themselves may be impacted by earthquakes or flooding. In the context of drone deliveries, a warehouse could suddenly become inaccessible. When this occurs, other bases/warehouses may need to cover a cell/building, even if they were previously not the closest base. Thus, it may be desirable to have multiple bases able to cover a given cell.

While this core approach offers a strong foundation, it's crucial to acknowledge the value of the more intricate formulations which are detailed in the aforementioned work. These advanced formulations provide a powerful set of tools for enhancing the redundancy of SAR plans. They enable the creation of alternative search patterns that can be seamlessly implemented if relocation becomes necessary.

2.1.3 Drone Delivery

The secondary case study we look at explores a method for simulating drone delivery demand within an urban environment. The demand generation approach we use leverages open-source geospatial and demographic data to construct a demand distribution across the city of interest. This generated demand will serve as a foundation for strategic decision-making regarding drone delivery network deployment. For example, it will help determine where to place warehouses (equivalent to bases in the SAR example) to house delivery operations while ensuring optimal placement near high-demand hotspots. Additionally, the relative demand between each building in different regions (equivalent to the search need probabilities in the SAR example) will add physical constraints on routing since drones can only carry some bounded number of packages in a single trip.

Data Acquisition and Processing: The algorithms for generating this dataset are from our collaborators at Purdue for a NASA ULI project [52]. OpenStreetMap (OSM) is the primary source for geospatial data, enabling the creation of a digital map of the target city (e.g., Austin). Buildings are identified on the maps through OSM and some are designated as potential depots/warehouse locations based on tags associated with them. Demographic

data, crucial for demand estimation, is selected from US Census Bureau data. This data is integrated with the geospatial information to create a comprehensive view of the urban landscape, including factors such as median household income and population density. Fig. 2.5 below shows these various metrics from the data at the census tract level overlaid on the Austin geography.

Demand Estimation Model: The demand estimation model assumes an S-shaped relationship between the number of packages ordered per month and the median household income of a specific area (see Fig. 2.6). This relationship reflects a natural saturation point as income increases and is modeled below (Equation 2.8):

$$f(x) = \frac{L}{1 + e^{-k(x-x_0)}} \tag{2.8}$$

A logistic function is used to account for the diminishing effect of increasing income on order frequency, capping the order potential in high-income areas. Population density is factored in by adjusting the capped order value with a density-dependent term. The resulting equation (Equation 2.9) estimates the adjusted order potential (λ) for a given location, considering both income ($f(x)$) and population density (D) where:

$$\lambda = f(x) \times (1 + \alpha \times D) \tag{2.9}$$

1. λ represents the adjusted order potential for a specific location
2. $f(x)$ signifies the logistic function output based on median income (x)
3. α denotes the population density factor
4. D represents the population density of the area

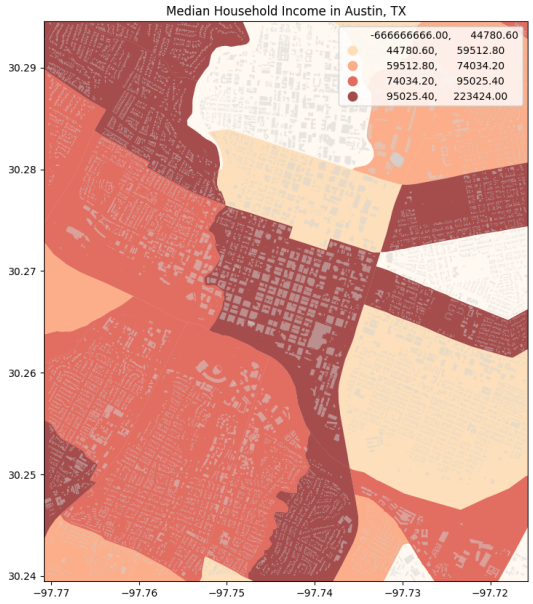

(a) Median Household Income

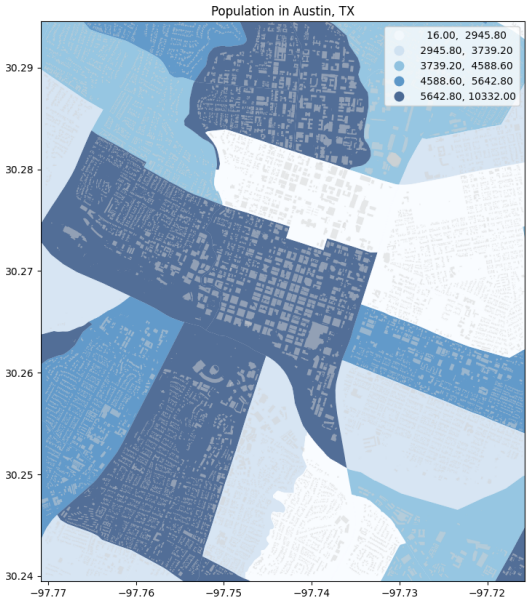

(b) Population Density

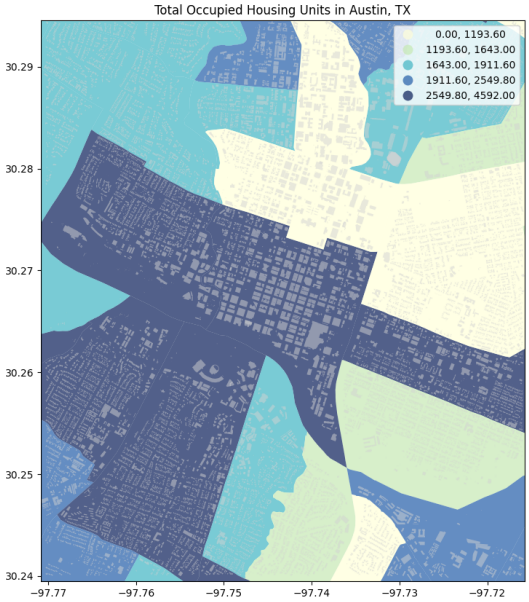

(c) Occupied Housing Units

Figure 2.5: Plots of various demographic factors on Austin, TX census tracts. Lighter colors indicate regions with lower package order likelihood. Each demographic is weighted differently to determine the underlying demand distribution across the city.

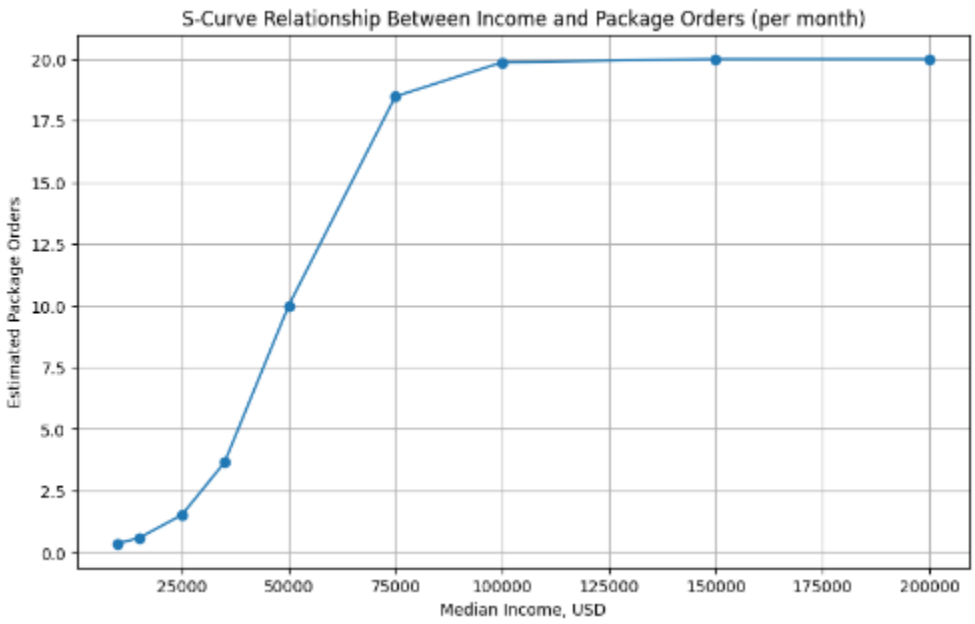

Figure 2.6: S-curve relationship estimated to relate median household income and an expected number of package orders on a monthly basis.

We convert the monthly estimate of orders to a daily rate for modeling purposes. This rate is then combined with a Poisson distribution to simulate the likelihood of a specific number of orders occurring within a day for each designated delivery location.

Underlying Assumptions: This model relies on several key assumptions. First, orders placed by different households are considered to be independent events. Second, the number of packages ordered per unit time follows a known average rate (λ), influenced by income and population density as described above. Finally, the Poisson distribution is assumed to effectively model the probable number of package orders (events) occurring in a fixed interval (daily in this case).

Identifying Delivery Depots: Minimizing setup costs is crucial for a successful drone delivery network. The first step of this model is to identify established infrastructure, such as supermarkets, convenience stores and department stores (e.g., Walmart, Target, CVS), as potential starting points (depots) for drone deliveries. These locations already possess the infrastructure for package handling, making them ideal candidates for depot integration. The model can be further expanded to incorporate new warehouse locations and other large

storage buildings within the city.

A simulated demand distribution across the chosen city is generated as shown in Fig. 2.7. Each building in the city is assigned a number of orders based on the factors discussed above. Using these values, we can now make informed decisions about depot locations and how to allocate resources.

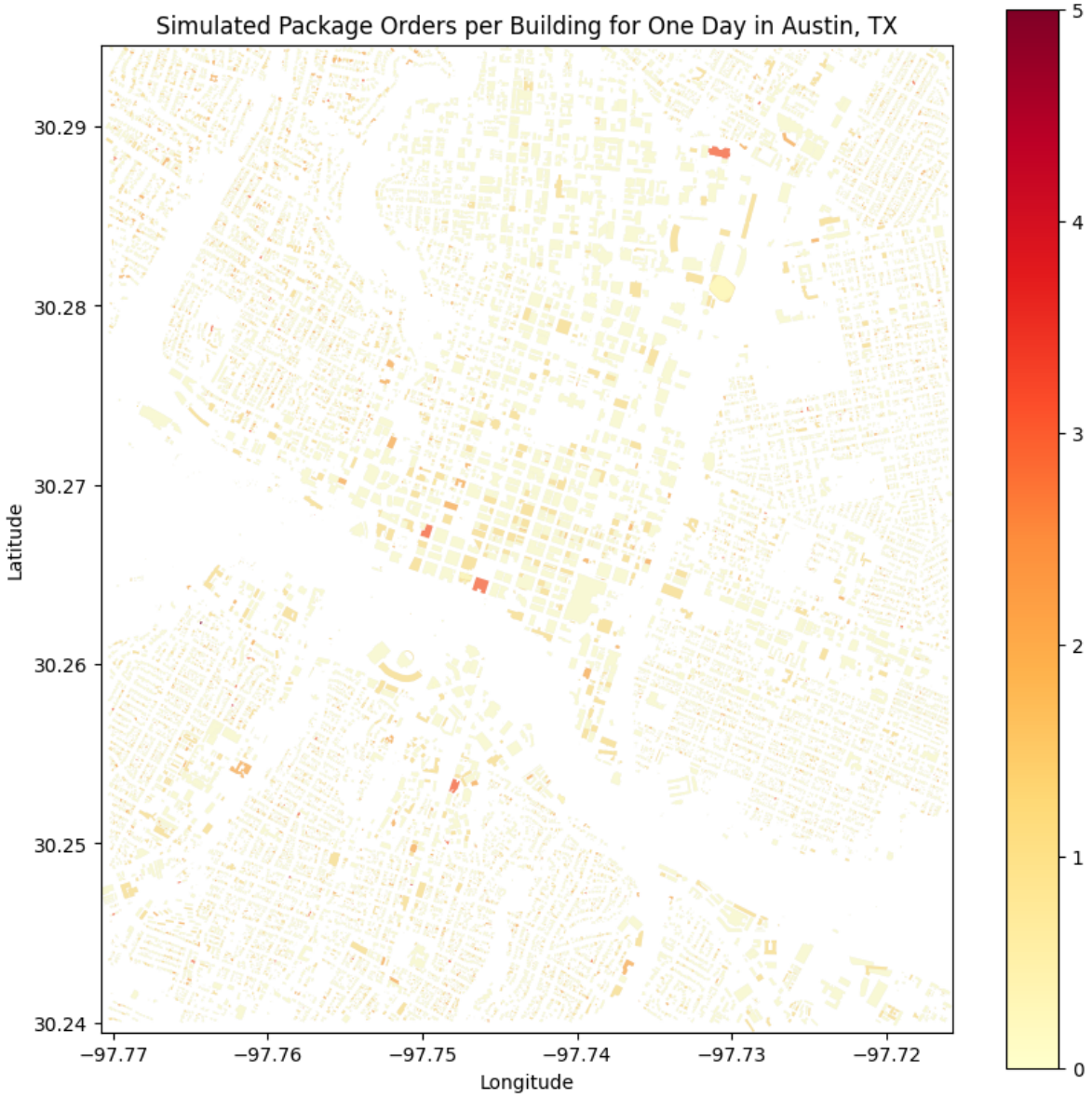

Figure 2.7: Single instance of simulated package demand across Austin, TX. Darker regions indicate more packages ordered (limited between 0 to 5 packages a day).

Chapter 3

Phase 2: Vehicle Routing

3.1 Problem Setup

The earlier parts of this thesis focus on the strategic placement of the bases for effective yet equitable coverage of a geographical region. The following sections focus on the vehicle routing component that aims to address the tactical part of search and rescue (SAR) operations and the actual delivery process. One possible goal is to minimize the resources (number of drones) needed to completely survey and/or service the region (given a set of energy constraints). Alternatively, one could determine the optimal allocation of a fixed number of drones across bases. Both these scenarios are considered below.

The routing process is local to each base and determined by using the base allocation procedure outlined in the previous sections. At a high level, cells in the geographical area are clustered based on the underlying search need. The result is a version of the traveling salesman problem (TSP), in which we search for the shortest possible routes between the clusters while satisfying the energy constraints of the drones being deployed.

After the initial exploration with the vanilla TSP, we used the Discounted Prize-Collecting TSP (D-PCTSP) as an alternative modeling technique to incorporate demand and enforce a prioritization in the visit order more effectively. The D-PCTSP offers greater flexibility in

accommodating diverse use cases compared to the vanilla TSP.

For the drone delivery scenario, we look into Capacitated Vehicle Routing Problems (CVRP) to account for realistic weight limits and the possibility of multiple package drop-offs at each location. While “demand" is not a crucial metric in the search phase of Search and Rescue (SAR) operations, CVRPs become highly relevant when modeling the rescue phase, where the “demand" at each node can represent the amount of resources that need to be sent to a location or the number of people that need to be airlifted from that location. Finally, we propose a modification to the PCTSP model that accounts for noise and privacy constraints (PA-PCTSP) by modifying the input data to distinguish regions that the drones can and cannot fly over.

3.2 Model Formulation

3.2.1 Vanilla Traveling Salesman Problem (TSP)

The idea of the traveling salesman problem is to find a tour of a given number of cities, visiting each city exactly once and returning to the starting city where the length of this tour is minimized. Below is the formulation for the routing optimization model:

Sets, Indices, & Parameters

L: set of locations $(0, 1, \ldots, n)$, where 0 is the index of the base and n is the number of cluster locations

D: set of drones $(0, 1, \ldots, K-1)$, where K is the number of drones

$i, j \in L$: indices of a specific location

$k \in D$: index of a specific drone

S_k: Tour of drone k (i.e. the subset of locations visited by that drone)

$t_{i,j} \in \mathbb{R}^+$: Travel time from location i to location j

$e \in \mathbb{R}^+$: Maximum distance (in km) that can be traveled by a drone with a single charge (energy constraint)

Decision Variables

$x_{i,j,k} = 1$ if drone k visits and goes directly from location i to location j; 0 otherwise

$y_{i,k} = 1$ if drone k visits location i; 0 otherwise

$z_k = 1$ if drone k is used; 0 otherwise

Objective Function

$$\text{minimize} \sum_{k=1}^{K} z_k \tag{3.1}$$

$$\text{subject to } y_{i,k} \leq z_k \quad \forall i \in L \backslash \{0\}, k \in D \tag{3.2}$$

$$\sum_{i \in L} \sum_{j \in L} t_{i,j} \cdot x_{i,j,k} \leq e \quad \forall k \in D \tag{3.3}$$

$$\sum_{k \in D} y_{i,k} = 1 \quad \forall i \in L \backslash \{0\} \tag{3.4}$$

$$y_{0,k} = z_k \quad \forall k \in D \tag{3.5}$$

$$\sum_{i \in L} x_{i,j,k} = y_{j,k} \quad \forall j \in L, k \in D \tag{3.6}$$

$$\sum_{i \in L} x_{j,i,k} = y_{j,k} \quad \forall j \in L, k \in D \tag{3.7}$$

$$\sum_{i \in L} y_{i,k-1} \geq \sum_{i \in L} y_{i,k} \quad \forall k \in D \text{ where } k > 0 \tag{3.8}$$

The input data for this model are base and cluster locations and the number of drones. The coordinates of each location are determined by the clustering step, and the Euclidean distance between each pair of locations is calculated and stored. We assume that the speed of the drone is 60 km/hr which is 1 km/min. Hence, travel time (in minutes) is equal to the distance (in km).

The decision variables determine the order in which each drone visits a subset of locations, which location is visited by each drone, and whether a given drone is used or not. We use two hierarchical objectives to optimize the routing. The primary objective (3.1) is to minimize the number of resources (i.e. drones) deployed from each base. The secondary objective, after minimizing the number of resources used, is to minimize the maximum of the time limit constraints. Constraint (3.2) ensures that for all locations other than the base (i.e. when $i = 0$), if the location is visited by drone k then drone k is indicated as being used (i.e. z_k is to 1). Constraint (3.3) ensures that no drone travels for more distance (and therefore time) than what the energy constraint e imposes, added as a slack variable. Constraint (3.4) enforces that each location is visited by exactly one drone (to ensure path efficiency). Constraint (3.5) enforces that the base (at location $i = 0$) is visited by every drone k that is used. We add constraint (3.6) for arrivals at a location, where if a location j is visited by drone k, then the drone came from some previous location i. We add a similar constraint (3.7) for departures from a location, where if drone k leaves location j, then the drone is going to another location i. Constraint (3.8) is used to break symmetry from a tour which can be traversed either clockwise or counterclockwise. Since we impose that the tour must start at the base ($i = 0$), we automatically remove symmetries of tours that contain the same order of locations but start and end at a different location (i.e. $0 \to 1 \to 2 \to 3 \to 0$ vs $2 \to 3 \to 0 \to 1 \to 2$).

3.2.2 Discounted Prize-Collecting TSP (D-PCTSP)

The main difference between the vanilla TSP and the prize-collecting TSP is that each location that can be visited by the vehicle has an associated “prize". The “cost" along the travel arcs are the distances travelled (and therefore representative of the battery consumption) which is the same as how we handle battery usage in the Vanilla TSP.

The new modification we introduce to the general PCTSP is a discount factor on the prize based on the time it takes to reach that node from the start of operation. In time-critical

applications, we want to enforce that travel order of the locations is important by strongly penalizing routes that reach people who are more severely affected later. Therefore, a harder to reach area with more affected people will be prioritized and will appear earlier in the trip even if that sacrifices some path efficiency. Here we emphasize providing equal access to search resources and focus less on the traditional optimization of variables like distance.

We maintain the mathematical formulation from the Vanilla TSP in Section 3.2.1, but add the following parameters to reflect the changes discussed above:

Additional Parameters

$p_i \in \mathbb{R}^+$: prize at location i

$\gamma \in (0, 1]$: decay factor to apply on each prize, scaled by the time to reach the prize

$c_{i,k} \in \mathbb{R}^{0+}$: time at which drone k arrives at location i, ($c_{i,k}$ can be arbitrary if drone k never arrives at location i)

Objective Function

$$\text{Primary: minimize} \sum_{i \in L} \sum_{j \in L} \left(t_{i,j} \sum_{k \in D} x_{i,j,k} \right) - \sum_{i \in L} \left(p_i \sum_{k \in D} y_{i,k} \gamma^{c_{i,k}} \right) \tag{3.9}$$

$$\text{Secondary: minimize} \sum_{k=1}^{K} z_k \tag{3.10}$$

Constraints

$$c_{i,k} \geq 0 \quad \forall i \in L, \forall k \in D \tag{3.11}$$

$$c_{j,k} \geq \sum_{i \in L} x_{i,j,k}(c_{i,k} + t_{i,j}) \quad \forall j \in L, \forall k \in D \tag{3.12}$$

We add new parameters to represent the prize p_i that can be collected at each location i as well as the decay factor γ that is set to a constant value for the entire routing operation. We also add a parameter $c_{i,k}$ to represent the time at which drone k arrives at location i. In this formulation, we use two hierarchical objectives to optimize the routing. The primary

objective (3.9) is to minimize the total route cost (i.e. distance traveled - accumulated revenue + fixed costs). If multiple feasible solutions get generated from the first optimization, then the secondary objective (3.10) is to minimize the number of resources deployed from each base. We also add two constraints on the new time parameter. Constraint 3.11 enforces that the time for a drone k to reach location i is always 0 or greater. Constraint 3.12 enforces that the elapsed time at the new location j is greater than or equal to the sum of the elapsed time at the previous location i and the time it takes to travel between locations i and j.

3.2.3 Capacitated Vehicle Routing Problem (CVRP)

The CVRP is also a relatively simple variant of the Vanilla TSP. The main difference is that there is a capacity constraint imposed on each drone. This is equivalent to a total number of packages or a certain weight it can carry during a single trip. Conditions on the battery life and energy consumption still hold but are not adjusted to account for the weight of the packages on-board (assuming constant discharge rate regardless of the total weight of the UAV and packages at a given time, which may not be realistic in practice). Note that locations with no demand are excluded from the list of locations and therefore excluded from any routing.

Depending on the resources available for a given base/depot, the outputted routes can be split between the vehicles (i.e they can be treated as multiple vehicles or multiple trips for a single vehicle).

This model aims to minimize total routing costs (battery consumption + fixed costs) and also minimize the number of routes. We add the following variables and constraints to the Vanilla TSP/VRP to reflect the capacity conditions discussed above in Section 3.2.1:

Additional Parameters

$q_j \in \mathbb{R}^+$: demand at location i

$Q \in \mathbb{R}^+$: capacity of each vehicle

Objective Functions

$$\text{Primary: minimize} \sum_{k \in D} \sum_{j \in L} \sum_{i \in L} t_{i,j} \cdot x_{i,j,k} \tag{3.13}$$

$$\text{Secondary: minimize} \sum_{k=1}^{K} z_k \tag{3.14}$$

Constraints

$$\sum_{i=0}^{n} \sum_{j=1}^{n} q_j \cdot y_{j,k} \leq Q \quad \forall k \in D \tag{3.15}$$

We add new parameters to represent the demand q at each location as well as the total capacity Q for each vehicle. In this formulation, we use two hierarchical objectives to optimize the routing. The primary objective (3.13) is to minimize the total route cost (i.e. distance traveled). The secondary objective (3.14), after minimizing the routing costs, is to minimize the number of resources (i.e. drones) deployed from each base. We also add the capacity constraint (3.15) that ensures that each vehicle only addresses as much demand in a single trip as it can carry. Note that with the current set up, the full demand at a node must be addressed (i.e. it cannot be split between multiple delivery vehicles). In the case that locations have more demand than the single carrying capacity of a drone, multiple points can be created to represent the same location and the demand can be split across these points.

3.2.4 Privacy Abiding (Capacitated) PCTSP (PA-PCTSP)

We introduce a new TSP variation that we call the Privacy Abiding Capacitated PCTSP which uses the PCTSP concept but adapts the input to impose constraints that ensure the models abide by privacy and noise restrictions that are put in place (particularly in urban environments). These no-fly zones are essentially buffers around certain buildings' footprints. In this model, we carry forward the parameters and constraints from the CVRP formulation in the previous section (3.2.3).

We can exploit the power of assigning a “prize" to locations on the map by associating a very large negative reward with the centroid of the building. However, this will only prevent the model from routing through the centroid and will not account for the rest of the area in the building footprint. To adjust for this we can fill the footprint with artificial locations that have 0 demand and large negative reward (these are added after the initial filtering of locations with no demand). We set these negative rewards such that the center of the building has the largest negative value and the value diminishes (becomes less negative) as you reach the outer borders of the footprint. This enforces a soft constraint instead of a hard no-fly constraint. Finally, we add a proxy point at the northwest corner (largest x and y coordinates in the extended geometry of the footprint). This proxy point is a replica of the building's original centroid (i.e. has the same prize associated with it).

Note that the actual formulation is quite similar to the one described in Section 3.2.2, with the exclusion of the decay factor as shown below:

Additional Parameters

$p_i \in \mathbb{R}^+$: prize at location i

Objective Function

$$\text{Primary: minimize} \sum_{k \in D} \sum_{j \in L} \sum_{i \in L} (t_{i,j} - p_j) \cdot x_{i,j,k} \tag{3.16}$$

$$\text{Secondary: minimize} \sum_{k=1}^{K} z_k \tag{3.17}$$

The primary objective (3.16) remains to minimize the total route cost (i.e. distance traveled - prizes collected + fixed costs). The secondary objective (3.17) also remains the same, minimizing the number of resources (i.e. drones) used at each base. Instead, the input data is modified to reflect the changes mentioned above. The implementation and validation of the PA-PCTSP model is not covered in this thesis and is a potential direction for future study.

Chapter 4

Case Studies

4.1 Search-and-rescue in Iwate, Japan

4.1.1 Methods

We start by populating a list of cells that require search resources by using the underlying search need probabilities or generated demand that we used to choose the optimal base locations (as explained in Section 2.1.1). Since the actual search need may differ from the prediction, we multiply each cell's original search need or package demand by a random sample drawn from a normal distribution. The ceiling of this product indicates the number of times the associated cell appears in the list. This list is then clustered with K-means clustering, where K is the number of clusters covered by a single base. Given the inclusion of repeated values to represent higher search needs, the clusters should reflect this higher need and will be more likely to be placed in vulnerable regions to guarantee coverage during routing. We add the base's coordinates to the list of cluster coordinates which will be passed into the respective routing model.

The main difference in the input between the Vanilla TSP and the PCTSP model is that each cluster has an associated "prize" that represents the number of people who are likely to be affected at that location (a scaled version of the search need probability) and is passed in

with the rest of the input. Below we detail the results of various parameter sweeps on the two model versions.

4.1.2 Vanilla TSP Results

First, we set the energy constraint to be a very large number (in this case 450 km/charge) to simulate the vanilla TSP problem. We use this situation as an opportunity to visualize the effect of varying the number of clusters per region serviced by a base. Fig. 4.1 visualizes simulations with 50 (Fig. 4.1a), 30 (Fig. 4.1b) and 20 (Fig. 4.1c) clusters.

(a) 50 Clusters (b) 30 Clusters (c) 20 Clusters

Figure 4.1: Impact of varying the number of clusters to route between in each base, under a large energy constraint of $e = 600$ km/charge. $P = 5, L = 45$ km.

Referring back to Fig. 4, all the colored regions will be covered during the routing phase as these clusters are distributed over the entire region. It is clear that having more clusters allows for better coverage of the area, and also more closely simulates the weaving of typical SAR routing patterns. Ideally, each cluster would represent all the cells in the field-of-view of a drone centered on the cluster, however, for ease of visualization and in the interest of running more simulations with reasonable computation times, we use $k = 30$ clusters for the remaining scenarios.

(a) $e = 450$ km/charge (b) $e = 300$ km/charge (c) $e = 150$ km/charge

Figure 4.2: Impact of varying the energy constraint e. $k = 30$. $P = 5, L = 45$ km.

The energy constraint (i.e. each drone's maximum flight time) is the most important parameter in this problem. Fig. 4.2 looks at the effect of varying the energy constraint (450 km/charge (Fig. 4.2a), 300 km/charge (Fig. 4.2b) and 150 km/charge (Fig. 4.2c)) while routing between the same $k = 30$ clusters with $P = 5, L = 45$ km. Specifically, we evaluate the coverage time, which is the time duration to visit all clusters, assuming all drones start at the same time. Table 4.1 shows the calculated coverage times for each energy constraint while using 1, 2, and 3 drones at each base. Depending on the number of drones at a base, the trips can be optimally assigned to each drone. If there is only a single drone at each base, then every trip is conducted by the same drone. The drone leaves the base, completes a trip, and returns to the base; then, it recharges for the next trip (with a 20% buffer) and sets out for the next trip. This process repeats until all the trips are complete. If there are multiple drones at each base, the idea is the same as above, except that some trips can run in parallel.

In this work, we assume that all maneuvers have the same discharge rate (i.e. takeoff, landing, cruising, turning, etc). Note that this is not entirely realistic, and could affect some planning decisions (i.e. the model may try to reduce the number of direction changes in

the path if turns consume more battery). Similarly, charge rates are usually slower than discharge rates. For simplicity, we will assume that charge and discharge rates are the same (i.e., it will take 100 minutes to charge for 100 minutes of flight). Including these modifications would simply require additional constraints in the linear program. Reducing the charge rate (thereby increasing charge time) compared to what is currently modeled would increase coverage time for scenarios that involve a single drone taking multiple trips.

Table 4.1: Coverage Time (in minutes) with Varying Energy Constraints and Drone Availability.

Energy Constraint (km/charge)	450	300	150
Coverage Time (min; 1 Drone)	326.02	424.12	639.33
Coverage Time (min; 2 Drones)	183.01	292.14	365.51
Coverage Time (min; 3 Drones)	128.67	177.99	148.26

We now elaborate on the coverage time calculations for multiple drones. When we have 1 drone at each base with $e = 450$ km/charge, since there is a single trip at each base, we simply take the maximum travel time across all the bases. In the case of 2 drones with $e = 450$ km/charge, we can split our single trip into two roughly equal-length trips that will be assigned to each drone. Here, we aim to minimize the time difference between the two sub-trips while ensuring the sub-trips still form feasible routes. We apply this procedure for any base that has more drones available than calculated routes. When $e = 300$ km/charge we note that there are some bases with a single trip and others with two trips. When we have a single drone servicing bases for two trips, it must return to recharge. The following expression calculates the total time for a single drone completing two trips, where a and b are the times for the first and second trips respectively and e is the energy constraint: $a+(b-(e-a))*1.2+b$. The middle term calculates the remaining charge after the first trip $(e - a)$ and determines how much additional charge is needed for the second trip $(b-(e-a))$ and adds a 20% charge buffer (multiplying by 1.2) to ensure that the drone doesn't return empty. The expression above simplifies to $2.2a + 2.2b - 1.2e$. When $e = 150$ km/charge we now have bases with either 2 or 3 routes. The total time calculation in the 3 trips + 1 drone case follows a similar

process to the 2 trips + 1 drone case. This time our expression has an additional variable c to represent the third trip and e_2 to represent the total charge before the second trip starts (an updated energy constraint): $a+(b-(e_1-a))*1.2+b+(c-(e_2-b))*1.2+c$, where $e_1 = e$ and $e_2 = (b-(e_1-a))*1.2+(e_1-a)$. This expression reduces to $1.96a+1.96b+2.2c-0.96e_1$. For the 3 trips + 2 drones case, we run the trip with the maximum length on one drone, and use the expression for 2 trips + 1 drone on the remaining two trips. Note that the same logic can be applied to cases with more tours or drones per base. As the energy constraint decreases, more trips/drones are required at each base to route between all the clusters. From an experimental perspective, the computation time increases significantly as the energy constraint decreases (as more options must be explored to find the optimal solution).

The second scenario we consider is how we can choose the best number of bases given a limited set of resources (in this case drones) that must be shared across all the bases. The following example assumes we have 6 drones to share across either 3 or 4 bases. Below, Fig. 4.3 shows both conditions.

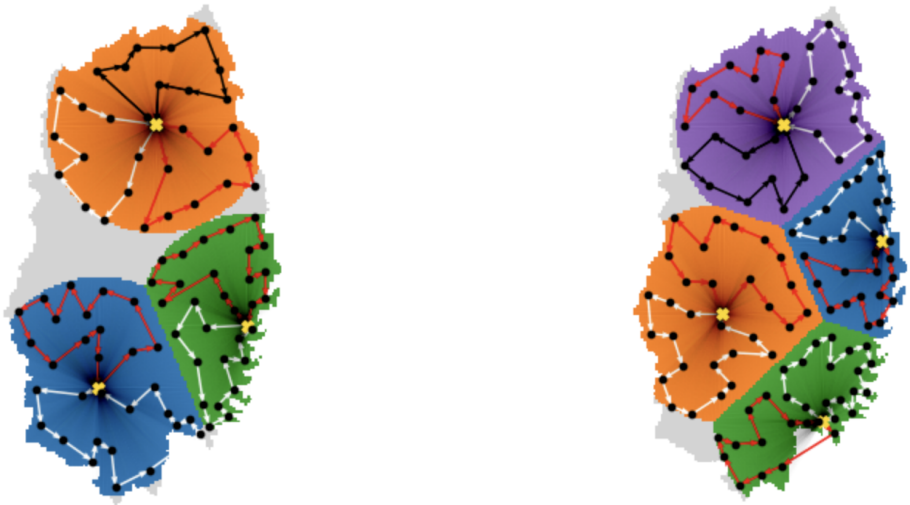

(a) 3 bases, Coverage Time = 452.96 (b) 4 bases, Coverage Time = 408.05

Figure 4.3: Impact of varying the number of bases. $k = 30$, $e = 200$ km/charge, $L = 45$ km.

We use the same calculation procedure detailed in the previous example. In the case of

3 bases, there are 2 bases with 2 trips and 1 base with 3 trips, so we assign 2 drones to each base. This results in a total coverage time of 452.96 minutes. In the case of 4 bases, we have 3 bases with 2 trips and 1 base with 3 trips. We can assign 1 drone to each of the bases with 2 trips and 3 drones to the base with 3 trips. Alternatively, we could assign 1 drone to the 2 bases with 2 trips and 2 drones to the remaining 2 bases. With the (1, 1, 1, 3) configuration we find that the coverage time is 603.78 minutes while with the (1, 1, 2, 2) configuration we find that coverage time is 408.05 minutes. In this example, a more distributed system (i.e. 4 bases with less resources at each) is faster and covers more cells than a more centralized system (i.e. 3 bases with more resources per base). This could be attributed to the fact that, even though the bases have the same radius ($L = 45$ km) and should cover approximately the same number of cells, spreading out the bases allows each base to address the most relevant clusters that are close to it instead of traveling to clusters that are far away just for the sake of coverage.

4.1.3 Discounted PCTSP Results

The unique parameter we explore in the D-PCTSP formulation is the γ factor that controls the decay on the prizes at each location. In the context of the SAR application this decay factor is extremely relevant as it should push the model to prioritize regions with higher search need and place them earlier in the route even if it results in minor path inefficiencies. Given the analysis in the previous section we only test the model on the $P = 5$ and $L = 45$km base configuration with 30 clusters at each base and an energy constraint of 150km/charge. We chose these values because the $P = 5$ and $L = 45$km base configuration has full coverage of the Iwate prefecture, using less than 30 clusters makes the simplified state space too sparse and more than 30 clusters becomes visually complicated to parse, and the 150km/charge constraint is closer to realistic bounds for fixed wing drone flight times.

In Figure 4.4 below we run analysis for γ values of 1, 0.9 and 0.8 across the same demand set for search around the Iwate Prefecture.

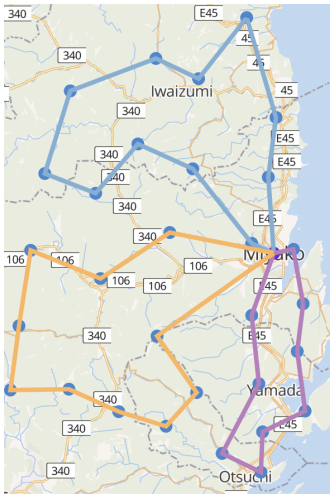

(a) Base=0, $\gamma = 1$

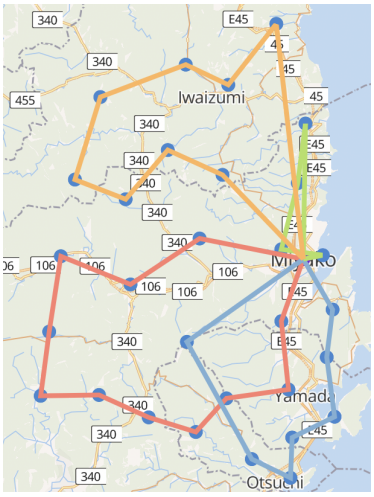

(b) Base=0, $\gamma = 0.9$

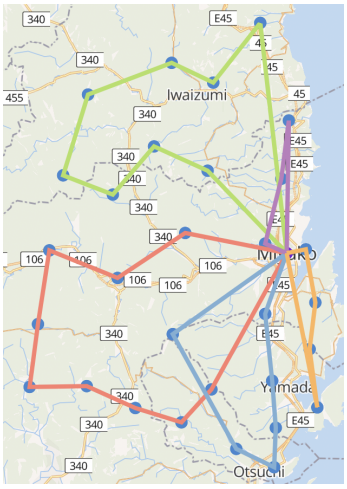

(c) Base=0, $\gamma = 0.8$

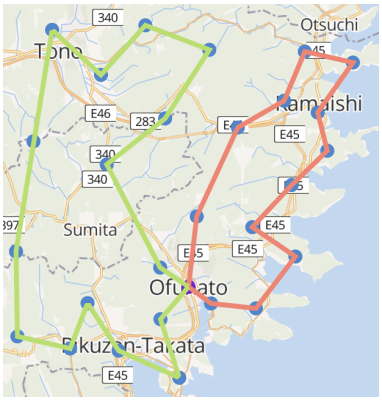

(d) Base=1, $\gamma = 1$

(e) Base=1, $\gamma = 0.9$

(f) Base=1, $\gamma = 0.8$

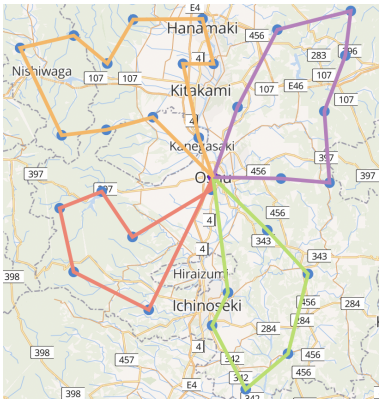

(g) Base=11, $\gamma = 1$

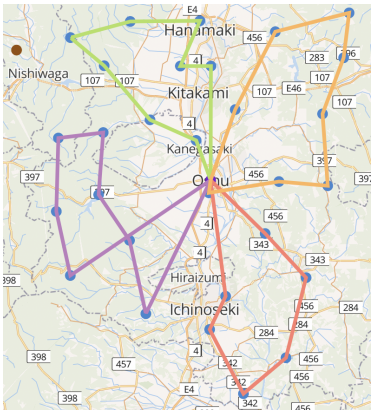

(h) Base=11, $\gamma = 0.9$

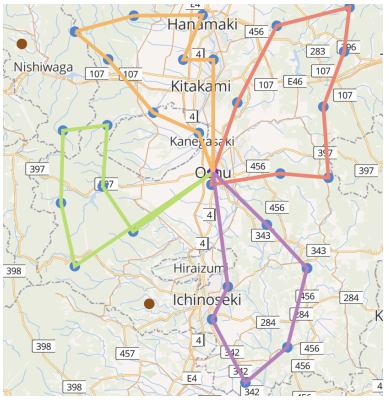

(i) Base=11, $\gamma = 0.8$

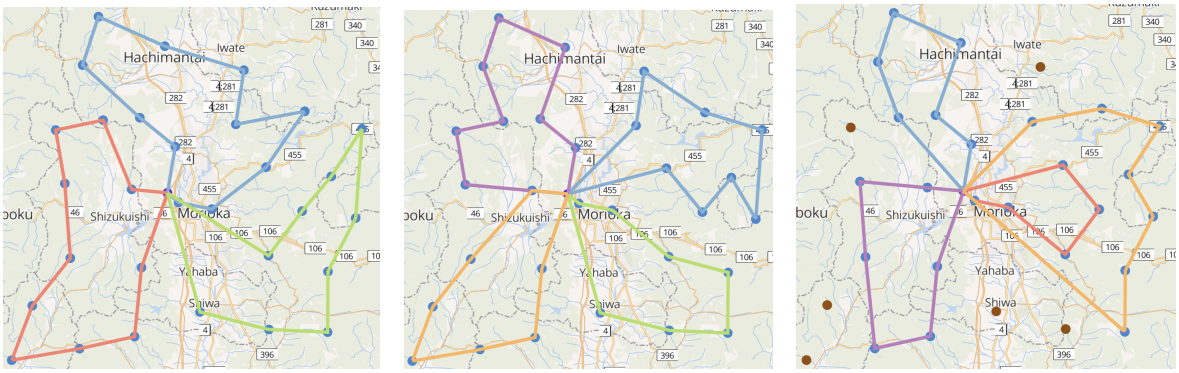

(j) Base=12, $\gamma = 1$ (k) Base=12, $\gamma = 0.9$ (l) Base=12, $\gamma = 0.8$

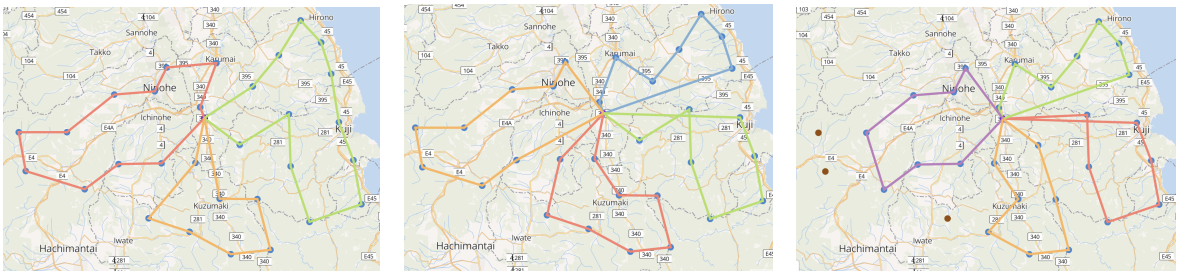

(m) Base=28, $\gamma = 1$ (n) Base=28, $\gamma = 0.9$ (o) Base=28, $\gamma = 0.8$

Figure 4.4: Effect of varying the decay factor (γ) over various established base locations on D-PCTSP generated routes for the same search need demand distribution.

Looking at subfigures 4.4a, 4.4d, 4.4g, 4.4j and 4.4m, we see that the generated routes are optimal - the paths do not cross over each other and they also use the minimal possible resources to route since time is not an explicit priority when $\gamma = 1$. This is also reflected in the distance travelled on each route. Looking at Table 4.2 we see that for $\gamma = 1$ most of the routes are flown to maximal battery usage (i.e. distances are ≥ 140 given the upper bounded 150km/charge energy constraint) while for $\gamma = 0.9$ and 0.8, none of the trips are more than 140km on a single charge.

Table 4.2: Individual Route Times (in minutes) with Varying γ Values From Output Routes in Figure 4.4.

Base #	$\gamma = 1$	$\gamma = 0.9$	$\gamma = 0.8$
0	132, 81, 138	134, 90, 49, 131	127, 85, 131, 41, 50
1	97, 148	49, 113, 121	53, 109, 93, 84
11	102, 97, 108, 144	97, 109, 136, 110	110, 116, 97, 109
12	138, 148, 150	131, 106, 116, 108	74, 91, 96, 140
28	141, 146, 105	108, 98, 123, 126	120, 98, 101, 92

When the decay factor is 1 we observe that the resulting routing is exactly what the Vanilla TSP formulation produces as seen in Figure 4.5. This is as expected as the decay multiplier is 1^d (where d is the distance traveled so far) and will always be 1, so there is no multiplicative penalty for visiting a certain location now or at a later time in the path. The accumulated prize will be the same regardless of the order of the locations in the path.

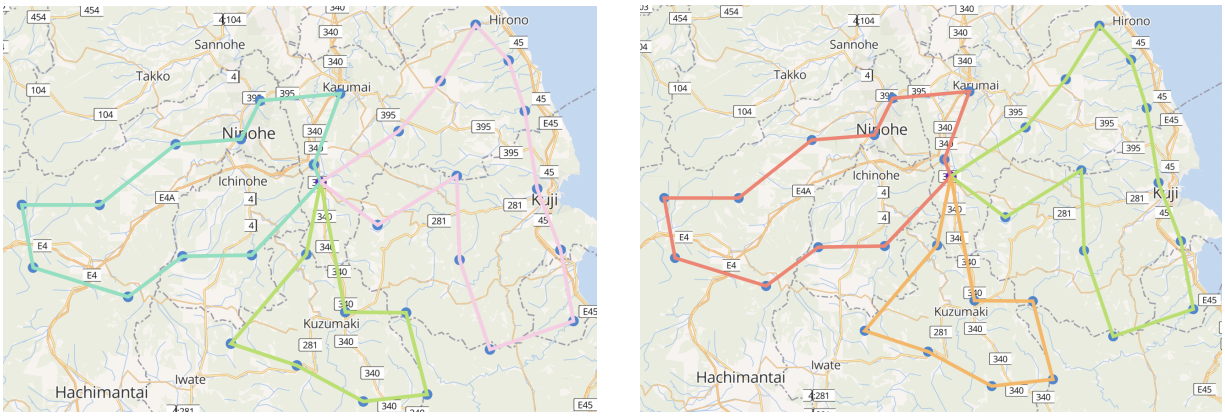

(a) TSP Routing for Base 28

(b) Discounted PCTSP Routing for Base 28

Figure 4.5: Comparing the output of the TSP and D-PCSTSP ($\gamma = 1$) routing models.

When we decrease the γ factor there are a few artifacts that manifest in the routing. Comparing the $\gamma = 1$ case to the $\gamma = 0.9$ case side by side for each base we see that some bases experience an increase in the number of routes required to best cover the region (4.4b, 4.4e, 4.4k, 4.4n). We also see some routes with lines that cross over each other within the route (4.4b, 4.4h, 4.4n). We have entire routes that overlap each other (4.4b, 4.4e). And we have routes that begin to ignore and not route to certain locations (4.4h). Further decreasing γ to 0.8, we see more overlapping routes (4.4c, 4.4f, 4.4l), crossovers (4.4c, 4.4f, 4.4i, 4.4o) and locations excluded from the routing (4.4i, 4.4l, 4.4o).

Looking back to Table 4.2 we see that as the γ factor reduces, the number of routes/vehicles required to service each base increases to reach the relevant regions with high search need sooner. This also results in many trips with shorter distances traveled (ex. 41 and 50 minute trips for Base 0 with $\gamma = 0.8$). Since we declare that costs associated with each flight are purely the charge times for each UAV we do not impose hard resource constraints in this

model version. If we wanted to more strongly enforce a limited number of UAVs at each base we could add a constraint to the formulation that restricted the number of trips or added a large fixed cost to activate a new trip. Implementing this resource restriction with three drones per base results in the route configurations shown in Figure 4.6 below.

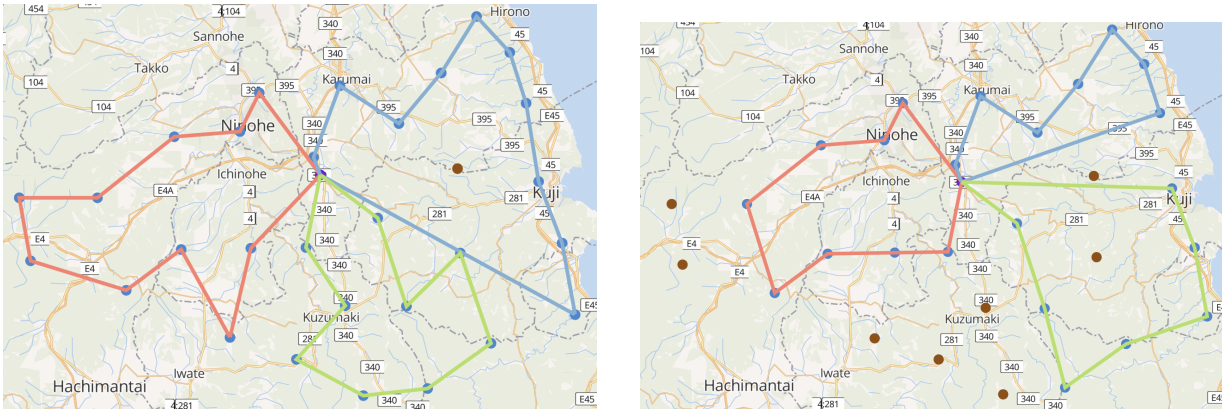

(a) $\gamma = 0.9$ (b) $\gamma = 0.8$

Figure 4.6: Comparing the effect of different γ values on outputted routes generated by D-PCTSP after restricting the number of drones available at each base to three.

We note that lower γ values (especially 0.8 and lower) require more resources otherwise it results in a significant number of locations that get excluded from the routing which is not ideal. Once an appropriate decay factor is determined, exploring the expected reward across different sets of conditions (number of bases, number of resources per base, etc) would help SAR operators conduct a tradeoff analysis as they consider what is relevant when designing missions. In Table 4.3 below, we compare the total reward accumulated in the routes generated by the Vanilla TSP and PCTSP models (accounting for decay at each location), restricted to at most four drones per base.

Table 4.3: Average Reward Collected with Varying γ Values From Output Routes in Figure 4.4.

Model	$\gamma = 1$	$\gamma = 0.9$	$\gamma = 0.8$
TSP	2131.4	489.48	197.17
PCTSP	2273.0	631.29	282.01

Comparing the TSP and D-PCTSP collected rewards, the D-PCTSP rewards are greater

than the TSP rewards across the board. For $\gamma = 0.9$ and 0.8 this pattern makes sense as the routes generated for D-PCTSP are designed to maximize reward and the outputted routes are significantly different from the TSP routes to account for the new priority of reaching higher rewards faster in the route. However, for $\gamma = 1$ the outputted TSP and D-PCTSP routes are the same (visually) yet their accumulated rewards are different. This is explained by the order of visit (clockwise vs counterclockwise). In the TSP model, there is no difference between traversing the route clockwise or counterclockwise. However, in the D-PCTSP model, the direction of traversal matters because in one configuration, the first location is first and in the other configuration it is the last. This will affect the decay applied to the prize at the location.

4.2 Drone deliveries in Austin, TX

4.2.1 Methods

We use the data collection process detailed in Section 2.1.3 to generate a demand simulation across the city and identify potential depots. We then use the base location algorithm described in Section 2.1.2 to identify how many and which of the potential bases to use as routing centers. Once these locations are selected we can separate all the locations with non-zero demand by the bases that can service them. We add the base's coordinates to the list of coordinates that represent each building with demand and pass it into the respective routing model.

The main difference between the SAR operations and drone deliveries is that each vehicle has a capacity which turns the Vanilla TSP model into Capacitated VRP model. Similarly, the PCTSP turns into a Capacitated PCTSP. In this case each location's "prize" is the simulated demand and each location with a privacy or noise constraint enforces a large negative prize at the location and uses a proxy point at the safe noise boundary to represent the original demand. These additional points are added to the input and are passed into the

PCTSP model. No decay factor is applied to the prizes in this version of the model.

Note that these models can also be applied to the rescue part of SAR operations. The delivery of rescue resources can be modeled like package deliveries or the airlifting of people can be treated like package pickups. Both of these scenarios still impose restrictions on the number of people that can be serviced.

4.2.2 CVRP Results

First, we explore the effective of carrying capacity on the routing results as this is the key parameter that differentiates the CVRP from the Vanilla TSP. In the context of drone deliveries, the carrying capacity can represent the weight of the packages a single UAV can carry. For simplicity, we assume that every package in demand has the same weight of one unit, so the capacity constraint enforces the number of packages that can be delivered in a single trip (leaving and returning to the depot). We ran the demand generation algorithm once and ran the base locating algorithm on this demand set to produce the demand distribution and base choices shown in Figure 4.7 below.

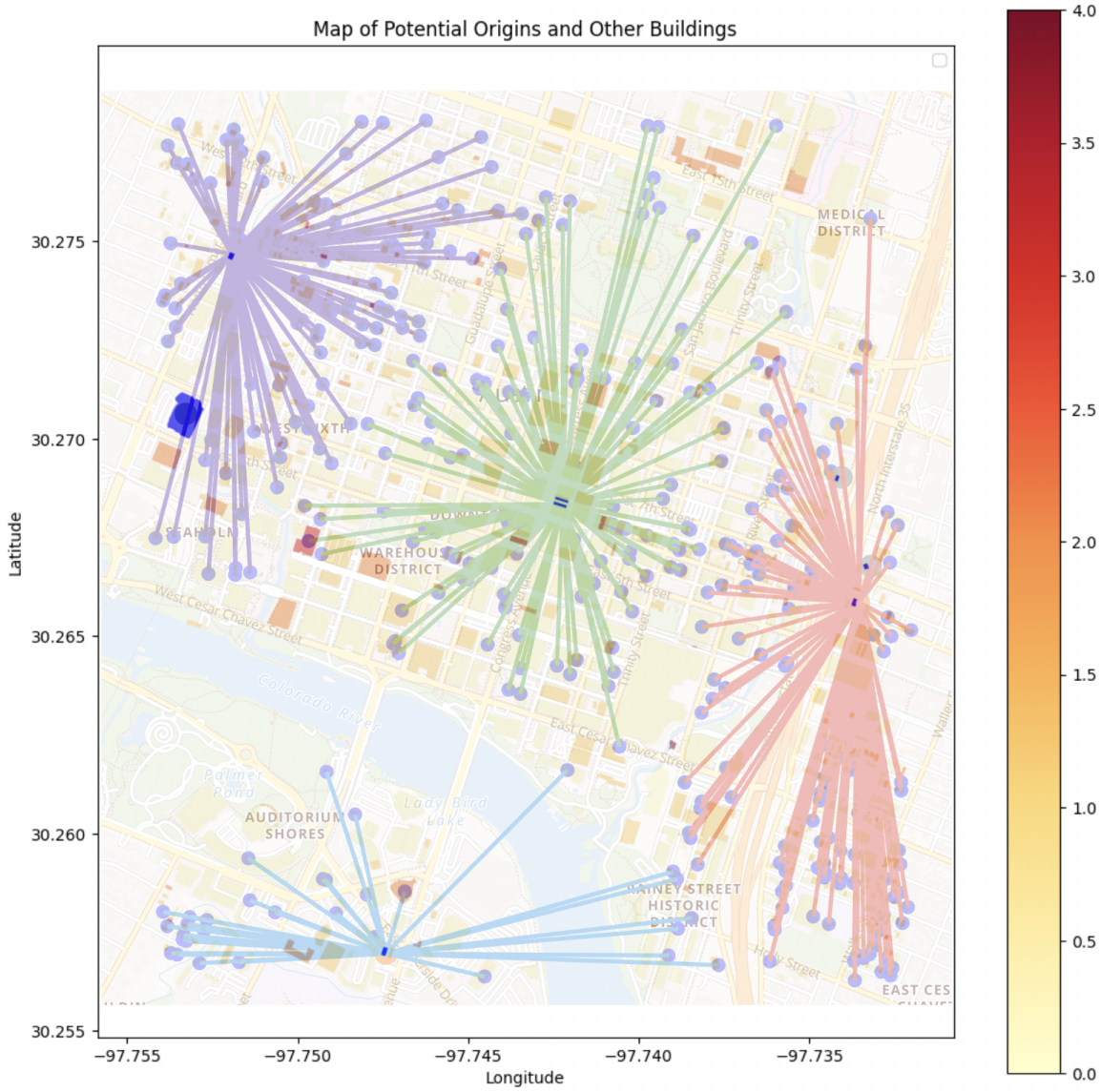

Figure 4.7: Demand locations matched with their associated bases based on proximity. Five of the potential bases were chosen based on the demand set.

In Figure 4.8 below, we run analysis for various carrying capacities c (specifically $c = 10$, 20, 40) using the demand set visualized above in Figure 4.7.

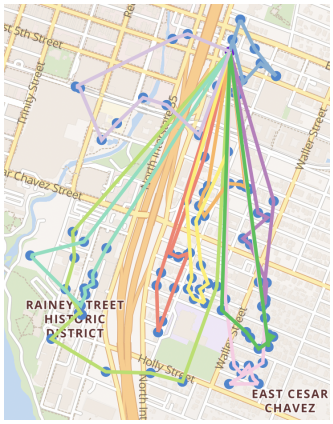

(a) Base=0, $c = 10$

(b) Base=0, $c = 20$

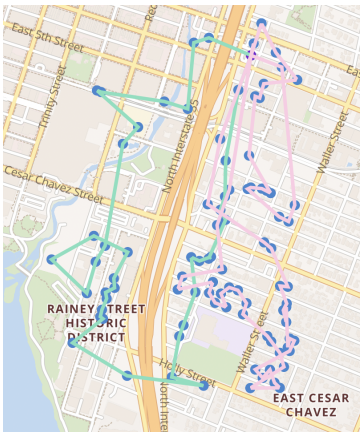

(c) Base=0, $c = 40$

(d) Base=2, $c = 10$

(e) Base=2, $c = 10$

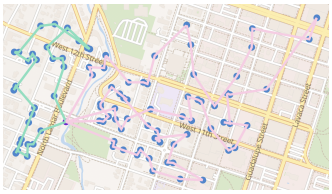

(f) Base=2, $c = 10$

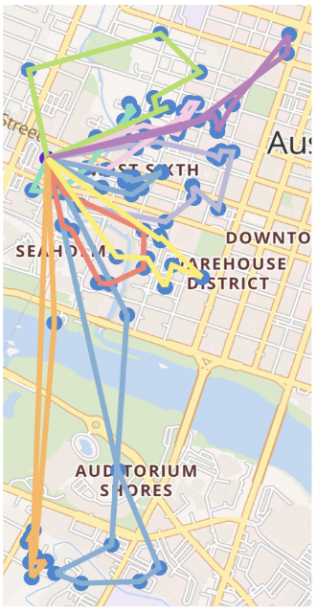

(g) Base=3, $c = 10$

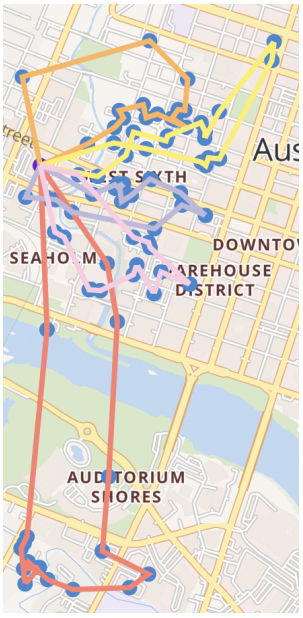

(h) Base=3, $c = 20$

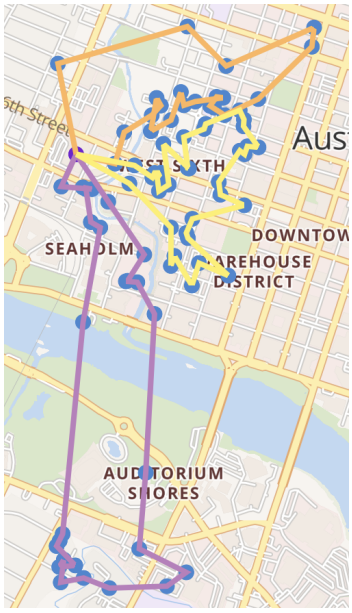

(i) Base=3, $c = 40$

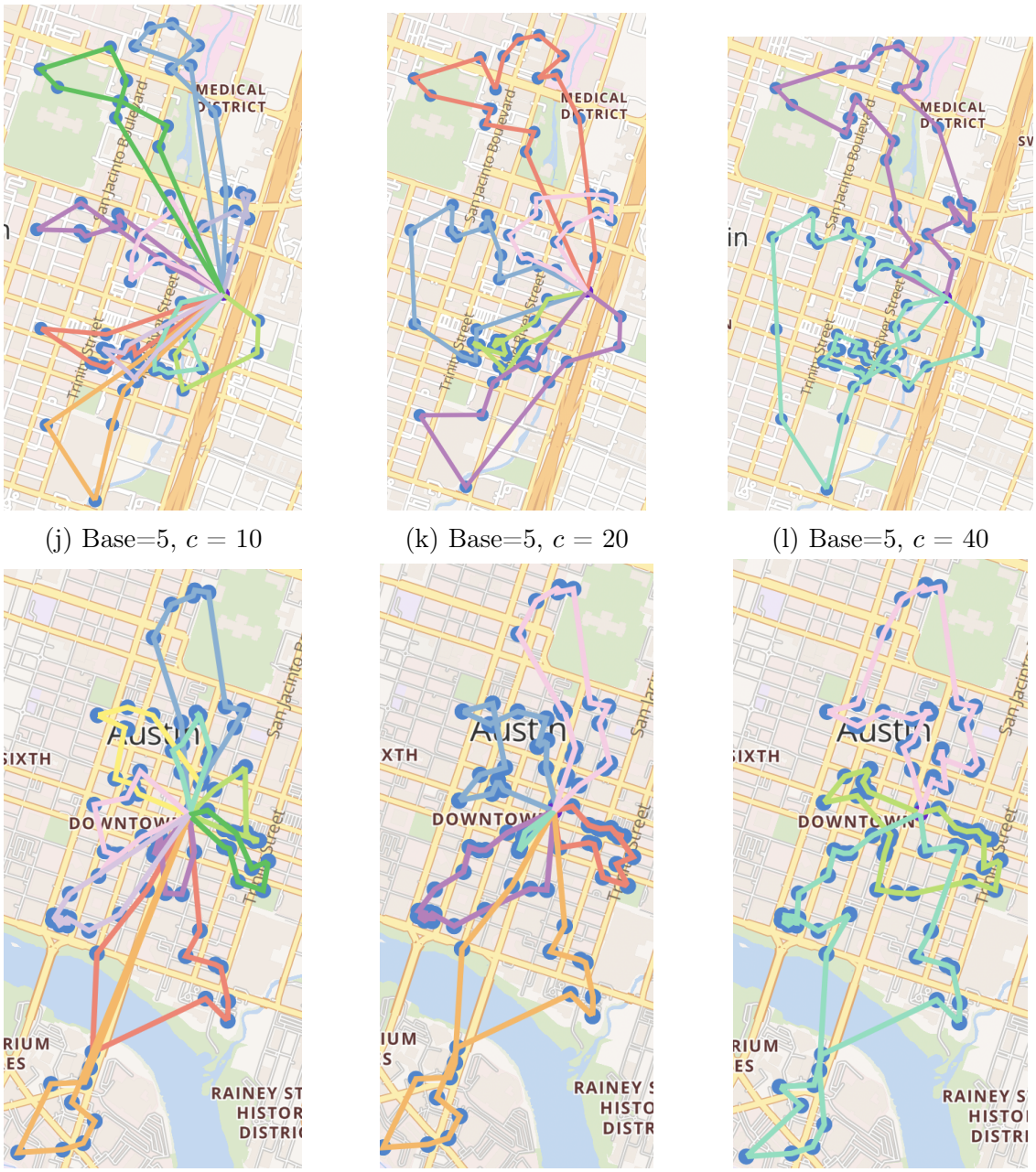

(j) Base=5, $c = 10$ (k) Base=5, $c = 20$ (l) Base=5, $c = 40$

(m) Base=6, $c = 10$ (n) Base=6, $c = 20$ (o) Base=6, $c = 40$

Figure 4.8: Effect of varying the carrying capacity (c) over various established base locations on CVRP generated routes for the same package demand.

Across the board most of the routes at each base have optimal routes (i.e. minimal crossovers and overlapping routes). However, we notice more of these features in the routes with a lower capacity constraint since varying demand at various locations can impact whether a single vehicle is able to service all the points in that subregion in the same trip.

Regions with more demand than a single drone can serve require more drones to travel to them to serve their needs (ex. 4.8a, 4.8b, 4.8g, 4.8j, 4.8k, 4.8m). A unique result of the CVRP model on this output that is different from plots we generated for the SAR scenarios is that many of the routes have long flight times to reach a large cluster of locations. Between these locations are short distances that the drones travel to address the pockets of demand. This can be seen in Figure 4.9 below where the left image is a route produced at one base and the right image is a representation of the distances traveled by each drone that is used. We can see that Drone 2 (orange) and 6 (pink) both cover long distances before dropping off packages in quick succession. These paths also overlap significantly as there are more points that need to be serviced in that region than can be serviced by a single drone. The other five drones are tasked to address closer clusters of demand locations.

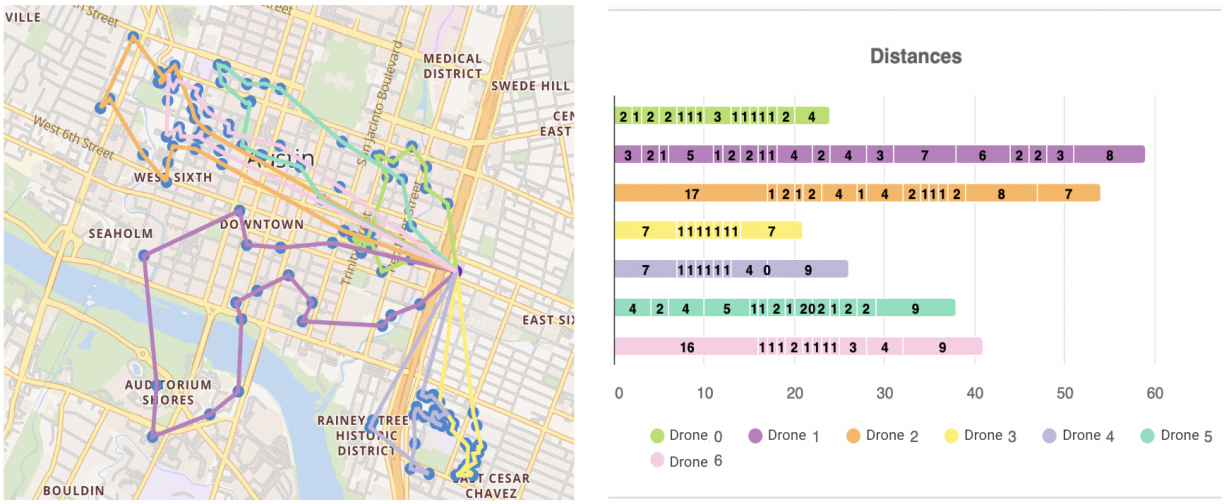

Figure 4.9: Routes with $e = 10$km, $c = 20$ (left) and distance traveled by each drone (right).

We see in Figure 4.10 below that with a very large capacity ($c = 500$) for the CVRP we produce the same route using the Vanilla TSP and the CVRP, which follows given that the only difference between the CVRP and Vanilla TSP is the capacity constraint. By imposing a capacity constraint larger than the total demand across all locations, we allow a single drone to carry all the demand, removing the intended effect of the capacity constraint.

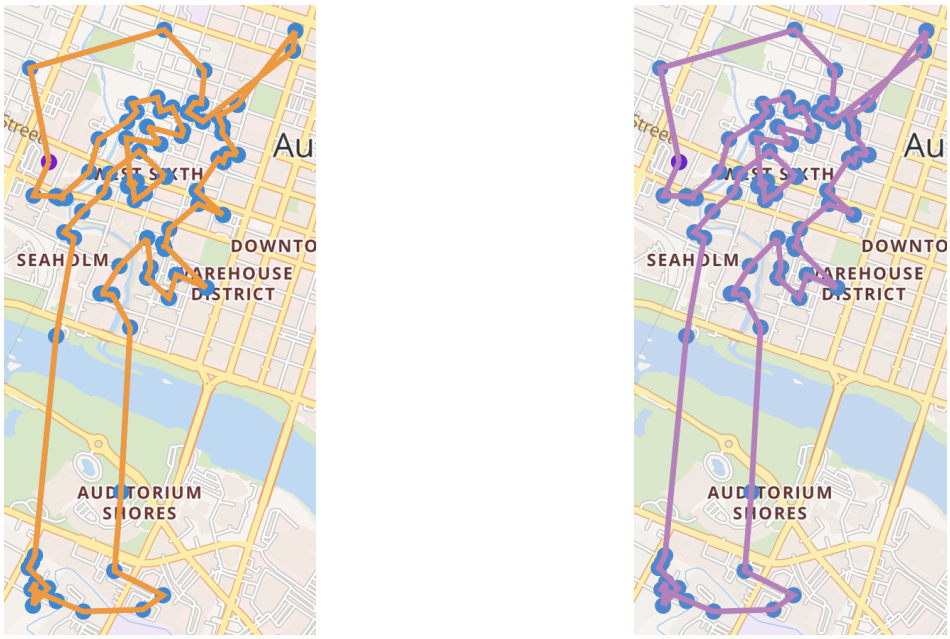

(a) TSP Routing for Base 3 (b) CVRP Routing for Base 3

Figure 4.10: Comparing the output of the TSP and CVRP ($c = 500$) routing models.

We can also examine the effect of changing the energy constraint on the generated routes. Figure 4.11 below examines energy constraints of $e = 5$, 10, and 20km for Base 3, where each vehicle has a carrying capacity 20.

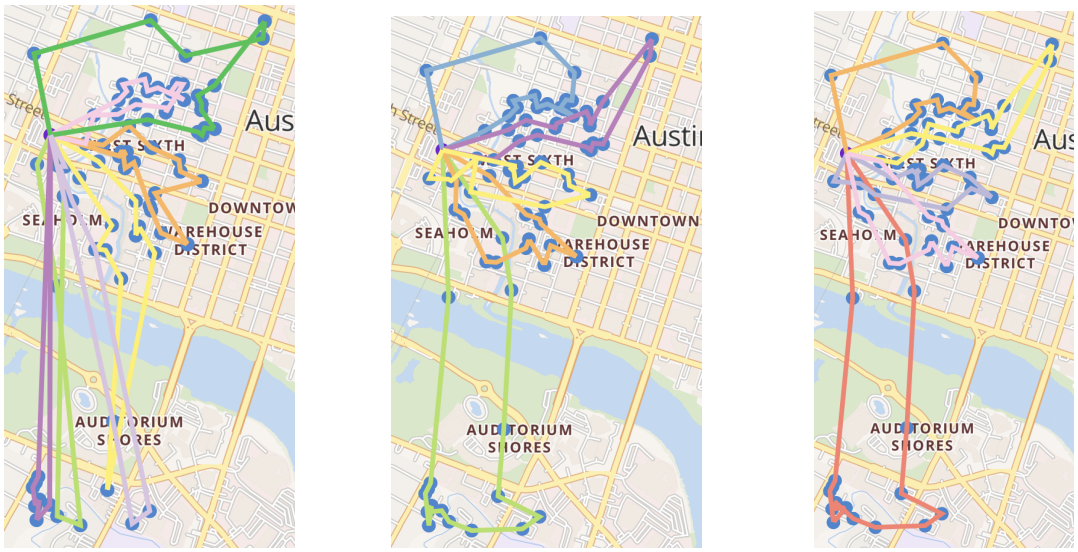

(a) $e = 3$ km (b) $e = 5$ km (c) $e = 10$ km

Figure 4.11: Comparing the effect of varying the energy constraints for each vehicle on the CVRP ($c = 20$) routing model for Base 3.

We notice that the routes produced with 5 and 10 km energy constraints are exactly the same (subfigures 4.11b and 4.11c) while the routes produces with a 3 km (subfigure 4.11a) energy constraint requires using two more drones. This result can be explained with the following dashboards in Figure 4.12 and Figure 4.13 that show the drone capacities (on the left) and distances traveled (on the right) by each drone.

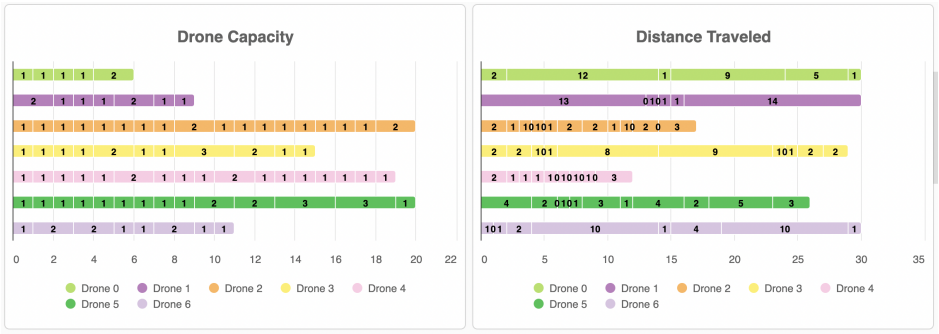

Figure 4.12: Used capacity (left) and distance traveled (right) by each drone with an energy constraint of 3 km.

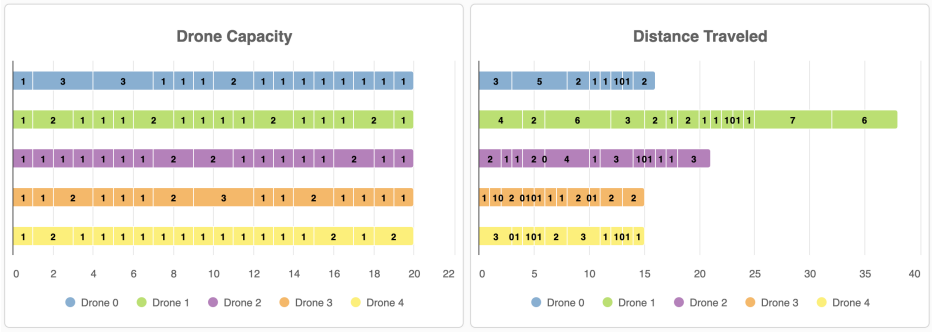

Figure 4.13: Used capacity (left) and distance traveled (right) by each drone with an energy constraint of 5 km.

We see that with the lower energy constraint of 3 km, there are more drones being used but very few of them actually reach full or close to full capacity. Instead, they all hit the maximum distance constraint. On the other hand, with the slightly larger energy constraint of 5 km, all the drones reach full capacity but very few of them utilize the full battery capacity available to them. As a result, increasing the energy constraint to 10 km does not change the output routes because the capacity constraint is the limiting factor for at least any scenarios with energy constraints of 5 km or greater.

Chapter 5

Conclusions

In the immediate aftermath of a disaster, it is important to quickly perform search and reconnaissance, followed by rescue operations. In this work, we focused on strategic base location, as it significantly influences the effectiveness of drone operations, and on tactical vehicle routing through case studies of search-and-rescue in the Iwate prefecture in Japan and drone deliveries in Austin, TX. We first generated search need probabilities and then tested a baseline formulation that tried to: (1) maximize coverage, and (2) minimize the distance between covered cells and their nearest base (DNB). The final component was incorporating tactical aspects of disaster response in the form of vehicle routing. Doing so allows us to evaluate metrics based on reconnaissance time which is essential for time-critical SAR operations.

We looked at variations of the Vanilla TSP problem for the various routing scenarios we explored. The Vanilla TSP works for best-case routing options and consistently provides the optimal solution for the search space. However, this is not realistic and reflective of underlying conditions in the real world. As such we explored the use of a Discounted Prize-Collecting TSP (D-PCTSP) model for the SAR case study where search need and demand was modeled as prize at each location and a discount was applied to each location based on the time it took for the vehicle to reach it in the path. We found that the D-PCTSP routing

had overall improvements in the total reward collected even with certain locations being excluded from the route. For the delivery case study we had to impose capacity constraints on the vehicles for each route, so we introduced the Capacitated Vehicle Routing Problem (CVRP). Finally, we began discussing a Privacy-Abiding Capacitated PCTSP model (PA-PCTSP) that could route accounting for noise and privacy constraints on certain buildings that would affect what regions the drones could fly as they complete deliveries.

For future work, we would implement and test the PA-PCTSP model with real privacy and noise constraints that are relevant to the Austin, TX metropolitan area. There also is an opportunity to revise some of the simplifying assumptions made in this work like making more realistic approximations of drone capacity, battery life, charge/discharge rates, etc. Additionally, considering operations with heterogeneous vehicle types (like crewed and uncrewed aircraft for search or trucks and UAVs for delivery) could further narrow the search space and more effectively use available resources. These studies could consider the different capabilities of crewed and uncrewed aircraft when locating bases for both classes of aircraft.

References

[1] World Meteorological Organization (WMO), *Weather-related disasters increase over past 50 years, causing more damage but fewer deaths*, 2011. URL: https://public.wmo.int/en/media/press-release/weather-related-disasters-increase-over-past-50-years-causing-more-damage-fewer.

[2] Z. W. Kundzewicz, S. Kanae, S. I. Seneviratne, *et al.*, "Flood risk and climate change: Global and regional perspectives," *Hydrological Sciences Journal*, vol. 59, no. 1, 2014. DOI: 10.1080/02626667.2013.857411.

[3] Institute for Water Resources (IWR), US Army Corps of Engineers), *Flood risk management approaches: as being practiced in Japan, Netherlands, United Kingdom and United States*, 2011.

[4] A. A. Ganin, E. Massaro, A. Gutfraind, N. Steen, J. M. Keisler, A. Kott, R. Mangoubi, and I. Linkov, "Operational resilience: Concepts, design and analysis," *Scientific reports*, vol. 6, 2016.

[5] J. Sublime, "The 2011 tohoku tsunami from the sky: A review on the evolution of artificial intelligence methods for damage assessment," *Geosciences*, vol. 11, no. 3, 2021, ISSN: 2076-3263. DOI: 10.3390/geosciences11030133. URL: https://www.mdpi.com/2076-3263/11/3/133.

[6] O. Fernandes, R. R. Murphy, J. Adams, and D. F. Merrick, "Quantitative data analysis: Crasar small unmanned aerial systems at hurricane harvey," *2018 IEEE International*

Symposium on Safety, Security, and Rescue Robotics (SSRR), pp. 1–6, 2018. URL: https://api.semanticscholar.org/CorpusID:52304331.

[7] T. Manzini, R. Murphy, and D. Merrick, "Quantitative data analysis: Crasar small unmanned aerial systems at hurricane ian," 2023. arXiv: 2308.14577 [cs.RO].

[8] E. Robinson, H. Balakrishnan, M. Abramson, and S. Kolitz, "Optimized stochastic coordinated planning of asynchronous air and space assets," *AIAA Journal of Aerospace Information Systems*, vol. 14, no. 1, pp. 10–25, 2017.

[9] S. Chowdhury, A. Emelogu, M. Marufuzzaman, S. G. Nurre, and L. Bian, "Drones for disaster response and relief operations: A continuous approximation model," *International Journal of Production Economics*, vol. 188, pp. 167–184, 2017, ISSN: 0925-5273. DOI: https://doi.org/10.1016/j.ijpe.2017.03.024.

[10] R. R. Murphy, *Disaster Robotics (Intelligent Robotics and Autonomous Agents series)*. The MIT Press, 2014.

[11] M. Viu-Roig and E. J. Alvarez-Palau, "The impact of e-commerce-related last-mile logistics on cities: A systematic literature review," *Sustainability*, vol. 12, no. 16, 2020, ISSN: 2071-1050. DOI: 10.3390/su12166492. URL: https://www.mdpi.com/2071-1050/12/16/6492.

[12] M. Turgut and B. Şeker, "Drone technology in transportation management: A systematic review and framework for future research," *Journal of Aviation*, vol. 7, no. 2, pp. 251–261, 2023. DOI: 10.30518/jav.1277694.

[13] J. Zhang, J. F. Campbell, D. C. Sweeney II, and A. C. Hupman, "Energy consumption models for delivery drones: A comparison and assessment," *Transportation Research Part D: Transport and Environment*, vol. 90, p. 102 668, 2021, ISSN: 1361-9209. DOI: https://doi.org/10.1016/j.trd.2020.102668. URL: https://www.sciencedirect.com/science/article/pii/S1361920920308531.

[14] H. Eskandaripour and E. Boldsaikhan, "Last-mile drone delivery: Past, present, and future," *Drones*, vol. 7, no. 2, 2023, ISSN: 2504-446X. DOI: 10.3390/drones7020077. URL: https://www.mdpi.com/2504-446X/7/2/77.

[15] C. Fehling and A. Saraceni, "Technical and legal critical success factors: Feasibility of drones & agv in the last-mile-delivery," *Research in Transportation Business & Management*, vol. 50, p. 101 029, 2023, ISSN: 2210-5395. DOI: https://doi.org/10.1016/j.rtbm.2023.101029. URL: https://www.sciencedirect.com/science/article/pii/S2210539523000871.

[16] R. E. Alfaris, Z. Vafakhah, and M. Jalayer, "Application of drones in humanitarian relief: A review of state of art and recent advances and recommendations," *Transportation Research Record*, vol. 0, no. 0, p. 03 611 981 231 209 033, 0. DOI: 10.1177/03611981231209033. eprint: https://doi.org/10.1177/03611981231209033. URL: https://doi.org/10.1177/03611981231209033.

[17] A. Balasingam, K. Gopalakrishnan, R. Mittal, M. Alizadeh, H. Balakrishnan, and H. Balakrishnan, "Toward a marketplace for aerial computing," in *DroNet 2021 – 7th ACM Workshop on Micro Aerial Vehicle Networks, Systems, and Applications*, 2021.

[18] A. Andreeva-Mori, J. Homola, M. Johnson, K. Kobayashi, Y. Okuno, and P. Kopardekar, "Integrated UAS trajectory optimization for disaster response reconnaissance missions," in *ICAS*, 2022.

[19] C. Chin, K. Gopalakrishnan, M. Egorov, A. Evans, and H. Balakrishnan, "Efficiency and fairness in unmanned air traffic flow management," *IEEE Trans. on Intelligent Transportation Systems*, vol. 20, no. 9, 2021.

[20] C.-F. Hsueh, H.-K. Chen, and H.-W. Chou, "Dynamic vehicle routing for relief logistics in natural disasters," in *Vehicle Routing Problem*, T. Caric and H. Gold, Eds., Rijeka: IntechOpen, 2008, ch. 5. DOI: 10.5772/5641. URL: https://doi.org/10.5772/5641.

[21] N. Roy, W. Burgard, D. Fox, and S. Thrun, "Coastal navigation-mobile robot navigation with uncertainty in dynamic environments," in *Proceedings 1999 IEEE International Conference on Robotics and Automation (ICRA)*, 1999.

[22] A. Balasingam, K. Gopalakrishnan, R. Mittal, V. Arun, A. Saeed, M. Alizadeh, H. Balakrishnan, and H. Balakrishnan, "Throughput-fairness tradeoffs in mobility platforms," in *ACM MobiSys 2021*, 2021.

[23] N. Hanlon, M. Kumar, and K. Cohen, "Neuro-fuzzy dynamic programming for decision-making and resource allocation during wildland fires," in *51st AIAA Aerospace Sciences Meeting Proceedings*, 2013.

[24] H. Balakrishnan and B. Chandran, "A distributed framework for traffic flow management in the presence of unmanned aircraft," in *Proceedings of the USA/Europe Air Traffic Management R&D Seminar*, 2017.

[25] L. Ozdamar, "Planning helicopter logistics in disaster relief," *OR Spectrum*, vol. 33, 2011.

[26] C. Boonmee, M. Arimura, and T. Asada, "Facility location optimization model for emergency humanitarian logistics," *International Journal of Disaster Risk Reduction*, vol. 24, pp. 485–498, 2017, ISSN: 2212-4209. DOI: https://doi.org/10.1016/j.ijdrr.2017.01.017.

[27] A. Verma and G. M. Gaukler, "Pre-positioning disaster response facilities at safe locations: An evaluation of deterministic and stochastic modeling approaches," *Computers & Operations Research*, vol. 62, pp. 197–209, 2015, ISSN: 0305-0548. DOI: https://doi.org/10.1016/j.cor.2014.10.006.

[28] R. Gopalan, "The aircraft maintenance base location problem," *European Journal of Operational Research*, vol. 236, no. 2, pp. 634–642, 2014, ISSN: 0377-2217. DOI: https://doi.org/10.1016/j.ejor.2014.01.007.

[29] C. J. Jagtenberg, M. A. Vollebergh, O. Uleberg, and J. Røislien, "Introducing fairness in Norwegian air ambulance base location planning," *Scandinavian Journal of Trauma, Resuscitation and Emergency Medicine*, vol. 29, 2021.

[30] B. Villarreal, E. A. Granda-Gutierrez, S. Lankenau, A. C. Bastidas, and A. Montalvo, "Decreasing ambulance response time through an optimal base location," in *Proceedings of the 2017 international symposium on industrial engineering and operations management (IEOM)*, 2017.

[31] M. S. Daskin, "A maximum expected covering location model: Formulation, properties and heuristic solution," *Transportation Science*, vol. 17, no. 1, pp. 48–70, 1983. DOI: 10.1287/trsc.17.1.48. eprint: https://doi.org/10.1287/trsc.17.1.48. URL: https://doi.org/10.1287/trsc.17.1.48.

[32] Q. Wang, R. Batta, J. Bhadury, and C. M. Rump, "Budget constrained location problem with opening and closing of facilities," *Computers & Operations Research*, vol. 30, no. 13, pp. 2047–2069, 2003, ISSN: 0305-0548. DOI: https://doi.org/10.1016/S0305-0548(02)00123-5. URL: https://www.sciencedirect.com/science/article/pii/S0305054802001235.

[33] N. Ha, M. Akbari, and B. Au, "Last mile delivery in logistics and supply chain management: A bibliometric analysis and future directions," *Benchmarking An International Journal*, vol. Ahead-of-print, Apr. 2022. DOI: 10.1108/BIJ-07-2021-0409.

[34] Q. Xie, X. Liu, and X. Yan, "Base station location optimization based on the google earth and acis," HCC 2016, pp. 487–496, 2016. DOI: 10.1007/978-3-319-31854-7_44. URL: https://doi.org/10.1007/978-3-319-31854-7_44.

[35] V. Silva, A. Amaral, and T. Fontes, "Sustainable urban last-mile logistics: A systematic literature review," *Sustainability*, vol. 15, no. 3, 2023, ISSN: 2071-1050. DOI: 10.3390/su15032285. URL: https://www.mdpi.com/2071-1050/15/3/2285.

[36] C. J. Jagtenberg, M. A. Vollebergh, O. Uleberg, and J. Røislien, "Introducing fairness in norwegian air ambulance base location planning," *Scandinavian journal of trauma, resuscitation and emergency medicine*, vol. 29, pp. 1–10, 2021.

[37] F. Ramjerdi, "Equity measures and their performances in transport," *Transportation Research Record*, 2006. DOI: 10.1177/0361198106198300110. URL: 10.1177/0361198106198300110.

[38] T. Langmyhr, "Managing equity: The case of road pricing," *Transport Policy*, vol. 4, no. 1, pp. 25–39, 1997. DOI: 10.1016/S0967-070X(96)00031-5.

[39] P. Decorla-Souza, "Income-Based Equity Impacts of Congestion Pricing," *Federal Highway administration*, 2008.

[40] J. Eliasson, "Is congestion pricing fair?" *Transport Policy*, vol. 52, pp. 1–15, 2016, ISSN: 1879310X. DOI: 10.1016/j.tranpol.2016.06.009.

[41] S. R. Middleton, *Discrimination, Regulation, and Design in Ridehailing*, Massachusetts Institute of Technology SM Thesis, 2018.

[42] K. Dorling, J. Heinrichs, G. G. Messier, and S. Magierowski, "Vehicle routing problems for drone delivery," *IEEE Transactions on Systems, Man, and Cybernetics: Systems*, vol. 47, no. 1, pp. 70–85, Jan. 2017, ISSN: 2168-2232. DOI: 10.1109/tsmc.2016.2582745. URL: http://dx.doi.org/10.1109/TSMC.2016.2582745.

[43] S. Meng, X. Guo, D. Li, and G. Liu, "The multi-visit drone routing problem for pickup and delivery services," *Transportation Research Part E: Logistics and Transportation Review*, vol. 169, p. 102 990, 2023, ISSN: 1366-5545. DOI: https://doi.org/10.1016/j.tre.2022.102990. URL: https://www.sciencedirect.com/science/article/pii/S1366554522003672.

[44] A. Oran, K. Tan, B. Ooi, M. Sim, and P. Jaillet, "Location and routing models for emergency response plans with priorities," in Jan. 2012, vol. 318, pp. 129–140, ISBN: 978-3-642-33160-2. DOI: 10.1007/978-3-642-33161-9_20.

[45] A. Otto, N. Agatz, J. Campbell, B. Golden, and E. Pesch, "Optimization approaches for civil applications of unmanned aerial vehicles (uavs) or aerial drones: A survey," *Networks*, vol. 72, no. 4, pp. 411–458, 2018. DOI: https://doi.org/10.1002/net.21818. URL: https://onlinelibrary.wiley.com/doi/abs/10.1002/net.21818.

[46] A. Thibbotuwawa, G. Bocewicz, G. Radzki, I. Nielsen, and Z. Banaszak, "Uav mission planning resistant to weather uncertainty," *Sensors*, vol. 20, p. 515, Jan. 2020. DOI: 10.3390/s20020515.

[47] Statistics Bureau of Japan, *2020 population census*, May 2022.

[48] Y. Wakatsuki and K. Lah, *3 nuclear reactors melted down after quake, japan confirms*, 2011. URL: http://www.cnn.com/2011/WORLD/asiapcf/06/06/japan-nuclear.meltdown/index.html.

[49] Y. Tsuji, K. Satake, T. Ishibe, T. Harada, A. Nishiyama, and S. Kusumoto, "Tsunami heights along the pacific coast of northern honshu recorded from the 2011 tohoku and previous great earthquakes," *Pure and Applied Geophysics*, vol. 171, no. 12, pp. 3183–3215, 2014. DOI: 10.1007/s00024-014-0779-x.

[50] *Japan damage could reach $235 billion, world bank estimates*, 2011. URL: https://latimes.com/business/la-fgw-japan-quake-world-bank-20110322,0,3799976.story.

[51] C. Chin, A. Saravanan, H. Balakrishnan, and A. Andreeva-Mori., "Strategic planning of aerial assets for disaster response: Enabling efficient and equitable access to drone-based search resources," *15th USA/Europe Air Traffic Management Research and Development Seminar (ATM2023)*, URL: https://par.nsf.gov/biblio/10429241.

[52] Z. Gao, J.-P. Clarke, J. Mardanov, and K. Marais, *Developing 3d virtual safety risk terrain for uas operations in complex urban environments*, 2023. arXiv: 2310.12349 [cs.CE].